NASA CR 167885

NASA

CHARACTERIZATION OF ADVANCED ELECTRIC PROPULSION SYSTEMS

PREPARED FOR
LEWIS RESEARCH CENTER
NATIONAL AERONAUTICS AND SPACE ADMINISTRATION
GRANT NAG 3-76

Final Report
May 1982

Pradosh K. Ray
Department of Mechanical Engineering
Tuskegee Institute
Tuskegee Institute, Alabama

1. Report No.	2. Government Accession No.	3. Recipient's Catalog No.
NASA CR 167885		

4. Title and Subtitle	5. Report Date
Characterization of Advanced Electric Propulsion Systems	May, 1982
	6. Performing Organization Code

7. Author(s)	8. Performing Organization Report No.
Pradosh K. Ray	
	10. Work Unit No.

9. Performing Organization Name and Address	11. Contract or Grant No.
Department of Mechanical Engineering Tuskegee Institute Tuskegee Institute, Alabama 36088	NAG 3-76
	13. Type of Report and Period Covered
12. Sponsoring Agency Name and Address	June 1, 1980-January 31, 1982
National Aeronautics and Space Administration Washington, D.C. 20546	14. Sponsoring Agency Code

15. Supplementary Notes

Grant Monitor--William Kerslake, NASA Lewis Research Center
Cleveland, Ohio 44135

16. Abstract

Characteristics of several advanced electric propulsion systems are evaluated and compared. The propulsion systems studied are mass driver, rail gun, MPD thruster, hydrogen free radical thruster and mercury electron bombardment ion engine. These are characterized by specific impulse, overall efficiency, input power, average thrust, power to average thrust ratio and average thrust to dry weight ratio. Several important physical characteristics such as dry system mass, accelerator length, bore size and current pulse requirement are also evaluated in appropriate cases. Only the ion engine can operate at a specific impulse beyond 2000 sec. Rail gun, MPD thruster and free radical thruster are currently characterized by low efficiencies. Mass drivers have the best performance characteristics in terms of overall efficiency, power to average thrust ratio and average thrust to dry weight ratio. But, they can only operate at low specific impulses due to large power requirements and are extremely long due to limitations of driving current. Mercury ion engines have the next best performance characteristics while operating at higher specific impulses. It is concluded that, overall, ion engines have somewhat better characteristics as compared to the other electric propulsion systems.

17. Key Words (Suggested by Author(s))	18. Distribution Statement
Electric Propulsion Mass Driver Rail Gun MPD Thruster Free Radical Thruster Ion Engine	Unclassified--Unlimited

19. Security Classif. (of this report)	20. Security Classif. (of this page)	21. No. of Pages	22. Price*
Unclassified	Unclassified	87	

* For sale by the National Technical Information Service, Springfield, Virginia 22161

NASA-C-168 (Rev. 10-75)

This Page Intentionally Left Blank

TABLE OF CONTENTS

This Page Intentionally Left Blank

LIST OF FIGURES

INTRODUCTION

The shuttle based space transportation represents a low cost means of access to geocentric space. This will encourage large scale utilization of space for various activities.[1-3] The shuttle is expected to form the basis of most of the earth orbital missions for at least the next few decades. This type of transportation is divided into two phases; a high thrust chemical boost phase from earth's surface to place the spacecraft into a low earth orbit (LEO) and subsequent transfer of the payload from LEO to a higher orbit.

All current space transportation systems derive their propulsive forces from chemical rocket engines. However, the quantities of chemical fuel which have to be carried to LEO together with the spacecraft are steadily increasing as a consequence of increasing payloads and increasing mission times. The interest in more efficient propulsion systems derives mainly from the desire of reducing the propellant mass relative to that of the payload.

The specific impulse of the chemical rockets is limited even for the most energetic propellant combinations to below 500 sec. Beyond this lies a variety of propulsion modes which promise a specific impulse measured in thousands of seconds. Many of them use electrical energy as input energy and by employing various methods convert part of the input energy into kinetic energy of the masses exhausted from the thrusters. These electric propulsion systems are distinguished by high exhaust velocities, low propellant consumption, low thrust and long operating times. However, after a spacecraft has been placed into a LEO by chemical rockets, high thrust levels are no longer a necessity. Hence, for

missions not impaired by trip times, low thrust electric propulsion system becomes a preferred candidate.

A number of ideas have been proposed on ways to convert the input electrical energy to kinetic energy of the exhaust beam. One propulsion device which is beyond performance verification stages and close to operational status is the mercury electron bombardment ion thruster.[4] Most of the others are still in the laboratory experiment or technical concept stages but a few of them show enough potential to be seriously considered. Some of them are:

1. Linear electromagnetic accelerator or mass driver.[5]
2. DC electric rail gun thruster.[6]
3. Magnetoplasmadynamic (MPD) thruster.[7,8]
4. Free radical thruster.[9]

We report here the results of a study made to establish the performance parameters of these advanced electric propulsion systems and compare them with those of the mercury electron bombardment thrusters. Due to lack of definite information about the operating characteristics and masses of most of the electric propulsion systems, only results of parametric nature are reported.

ELECTRIC PROPULSION SYSTEMS

There are basically two different propulsion modes that can be used for upper stage transportations. These are:

1. High thrust chemical propulsion systems to effect orbital transfers in short periods of time (less than a day).
2. Low thrust electric propulsion systems for longer trip times.

High thrust chemical propulsion systems are needed to transfer personnel and priority cargo between orbits. They can make the transfer between LEO and GEO in about half a day or less which allows unshielded transit through the Van Allen radiation belts. Orbital transfer vehicles using chemical rocket engines require about 3 kg in LEO to place 1 kg of payload in GEO.[10]

Low thrust electric propulsion systems have high propulsive performance with specific impulses of 1000 sec and beyond. Thus, they would require less propellant to perform the same mission. A smaller fuel requirement is always desirable but since this propellant must be delivered from the earth this reduces the overall transportation cost considerably. This is significant, because earth to LEO transportation cost is a major portion of the overall mission cost.

Unlike the chemical rockets where the propulsive energy is contained in the propellant itself, the electric propulsion systems are characterized by an energy source independent of the impulsive mass. Due to the independent energy source, there is no inherent limitation of the specific impulse obtainable from an electric propulsion system. However, for a given thrust the propellant mass is reduced inversely

with increasing exhaust velocity, whereas the power and hence, the power-plant mass increase linearly with increasing exhaust velocity. The optimum specific impulse of an electric propulsion system is determined by the characteristic requirements of a specific mission.

Since the source of energy is not contained in the propellant in an electric propulsion system, there are necessarily a number of conversion steps between the primary energy source and the ejected reaction mass as compared to chemical rockets. Some energy is dissipated in each conversion step and this requires that as few conversion steps be incorporated in the propulsion system as possible. Also, each step in the conversion process must be highly efficient to ensure that the kinetic energy of the expelled propellant is not significantly less than the energy output of the power plant.

The conversion of the input electrical energy to the kinetic energy of the ejected propellants can be performed by employing a variety of physical principles. The propulsion systems investigated have thrusters where,

1. the principle of linear synchronous motors and dynamic magnetic levitation are used for acceleration of macro-particles in carriers containing superconducting coils (mass driver).

2. reaction masses are accelerated between parallel rail electrodes by the Lorentz force derived from passing a direct current through the rails (electric rail gun thruster).

3. an energy storage system drives a large current through a flowing gas creating a plasma which is accelerated via the Lorentz force generated by the interaction between the arc current and its self-generated magnetic field (MPD thruster).

4. free radicals are generated by using microwave energy to dissociate hydrogen and recombining and expelling them as exhaust beams (free radical thruster).

5. electrostatic forces are used to accelerate positive ions of mercury generated by passing an electric arc through mercury vapor (mercury electron bombardment ion thruster).

SYSTEM DESCRIPTION

Each system is briefly described in this portion. Readers are referred to appropriate references for information on designs, performances and mission characteristics.

Mass Driver[5,11-14]

The mass driver is a linear electromagnetic accelerator capable of launching reaction masses when designed as a rocket engine. Cylindrical buckets with superconducting coils carrying payloads are accelerated inside a coaxial assembly of drive coils several kilometers long. The payload is released after the desired velocity is achieved and the bucket is decelerated and returned to the starting position along a return track to be used again.

This device behaves essentially as a linear synchronous ac motor. The accelerating force is generated by a travelling magnetic field interacting with a magnetic dipole. The bucket is supported and guided without physical contact with the drive coils by dynamic magnetic levitation.

A small number of drive windings contained in one sector are excited at any given time to minimize power dissipation. A capacitor bank in each sector discharges current through feeders and through silicon-controlled rectifiers (SCR) to the drive windings. A schematic diagram of a mass driver reaction engine is provided in Fig. 1.

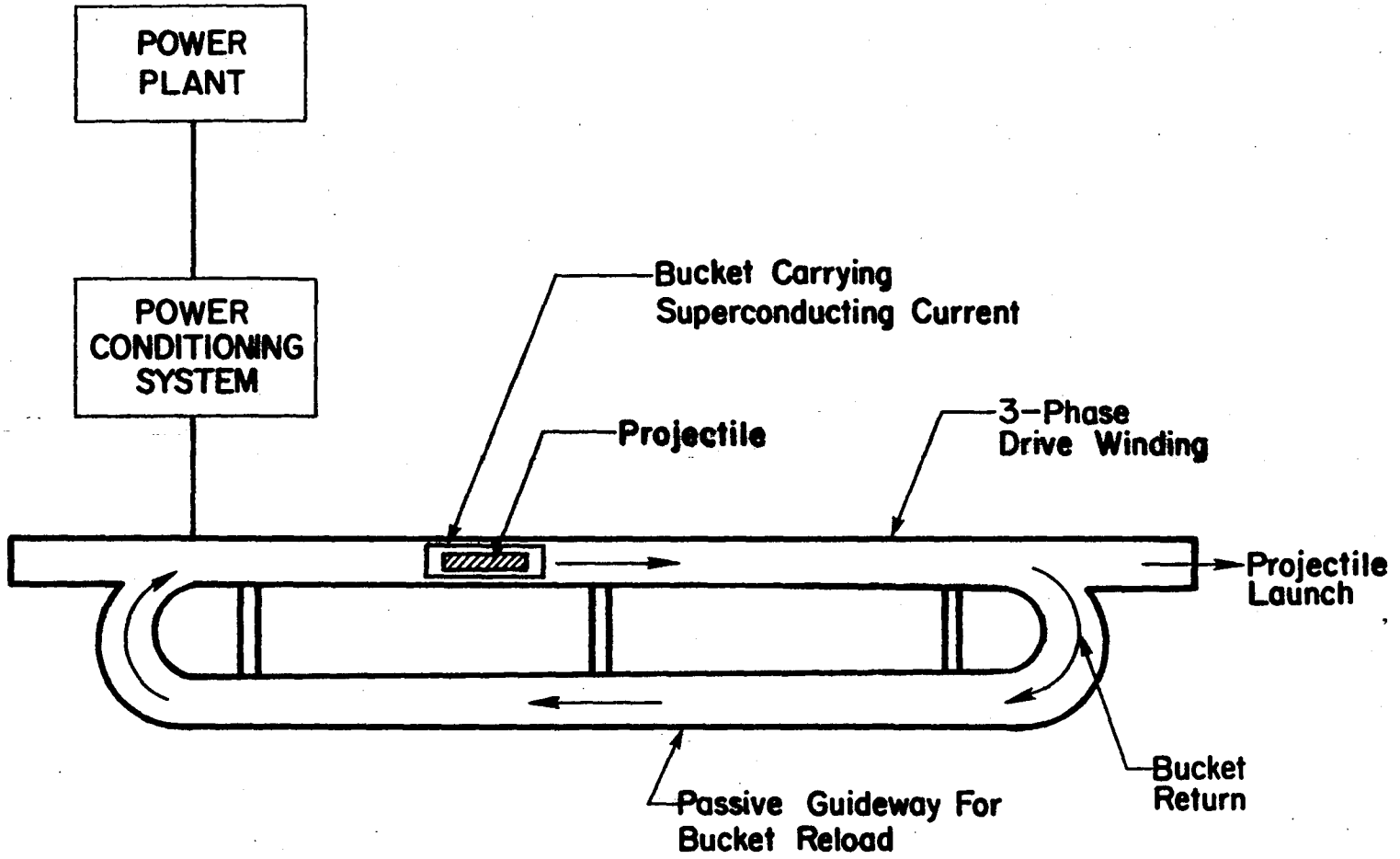

Figure 1. Schematic Diagram of a Mass Driver Reaction Engine.

Rail Gun Thruster[6,15-20]

The rail gun consists of a pair of parallel conductors separated by a distance and connected by a movable conductor. A large current (kiloamperes) flows in a short burst from one rail to the interconnecting conductor to the other rail. The interconnecting conductor is normally a thin metallic fuse which becomes a plasma when the large current is discharged through it.

The rail gun functions essentially as a linear dc motor. The plasma behaves as an armature while the parallel rails serve as a single turn field winding in series with the armature. The current $\underline{J}$ flowing in the rails generates a magnetic field $\underline{B}$ between the rails and this magnetic field interacts with the current flowing in the armature. The resulting Lorentz force ($\underline{J} \times \underline{B}$) acting on the armature accelerates the plasma along the rails. If the plasma is confined behind a projectile made of dielectric materials, the pressure of plasma will accelerate the projectile along with the plasma. The confinement of the plasma can be provided by the conducting rails on two sides and the dielectric materials on the other two sides. The peaking loads are supplied from a capacitor energy storage system and the current is discharged through a pulse shaping network containing an inductor. Fig. 2 shows a schematic drawing of a rail gun thruster.

MPD Thruster[8,21-24]

The self-field MPD thruster consists of a discharge chamber made of an annular anode ring and a centrally located cathode. After a suitable gaseous propellant, such as argon, is injected into the discharge

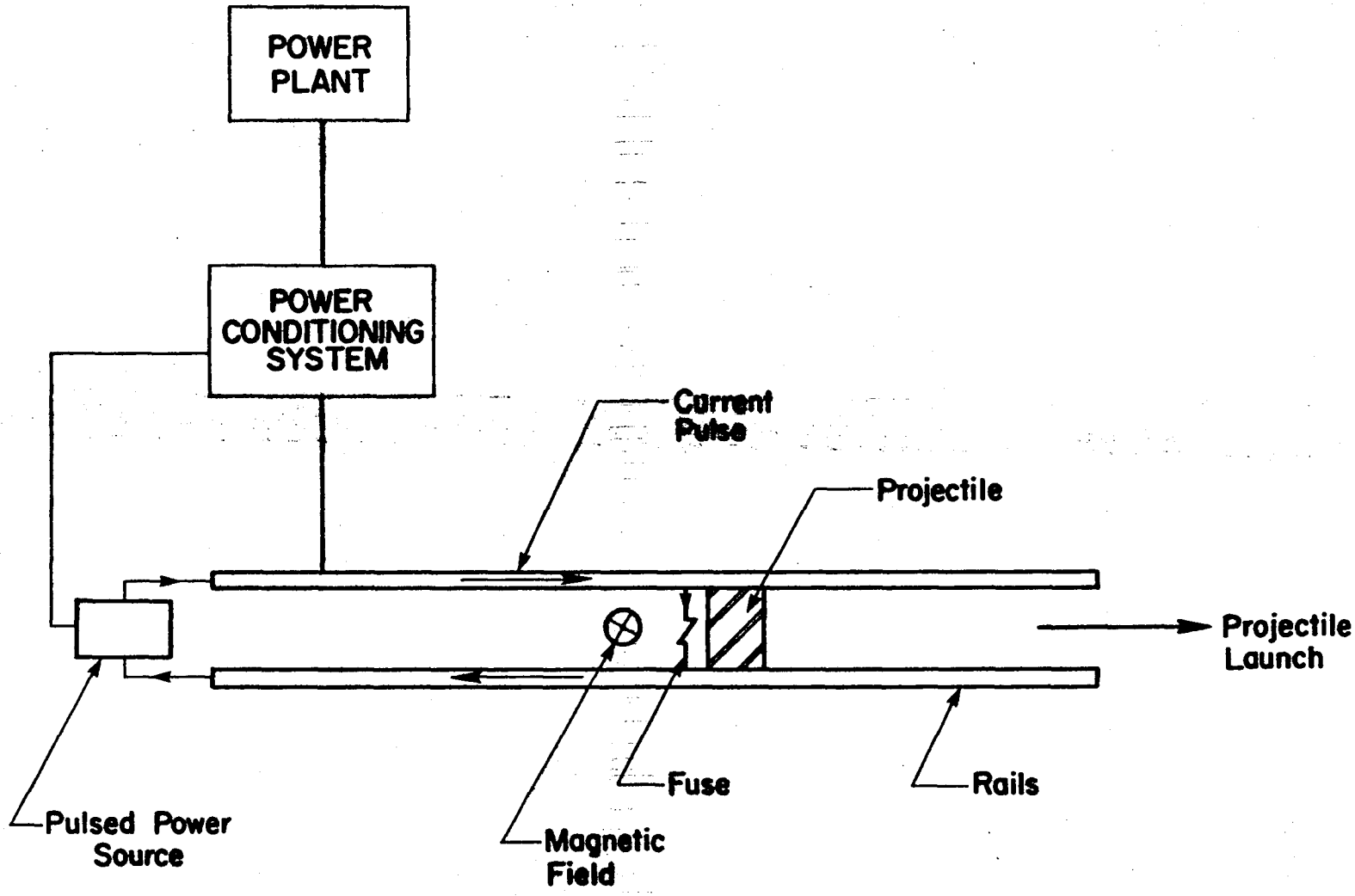

Figure 2. Schematic Diagram of a Rail Gun Thruster.

chamber, a large current pulse (kiloamperes) is passed from the anode to the cathode ionizing the propellant. A magnetic field $\underline{B}$ is induced inside the discharge chamber by this azimuthally symmetric current flow. It interacts with the current $\underline{J}$ to induce a Lorentz body force ($\underline{J} \times \underline{B}$) on the propellant gas. This Lorentz body force has an axial component which moves the plasma downstream and a radially inward component which confines the plasma. The plasma expelled from the discharge chamber provides the thrust.

The self-field MPD thruster is a low voltage (hundreds of volts), high current device which is well suited for operation in an intermittent, quasi-steady mode. A schematic drawing of a MPD thruster is shown in Fig. 3.

Free Radical Thruster[9,25,26]

This device operates on the principle of continuous creation of atoms dissociated from molecules of light gases, such as hydrogen, and recombining them in a chamber to obtain the heat of recombination of free atoms. The free radical thruster represents the ultimate chemical system yielding the highest specific impulse for one hundred percent dissociation and recombination.

The input electrical energy is converted to microwave radiation and fed into a resonant cavity. Molecular hydrogen gas flows through the cavity and a fraction of the molecules are dissociated by the microwave energy. The mixture of molecular hydrogen and dissociated hydrogen atoms then flows out of the cavity into a recombination chamber where the hydrogen atoms recombine releasing the energy absorbed in dissociation

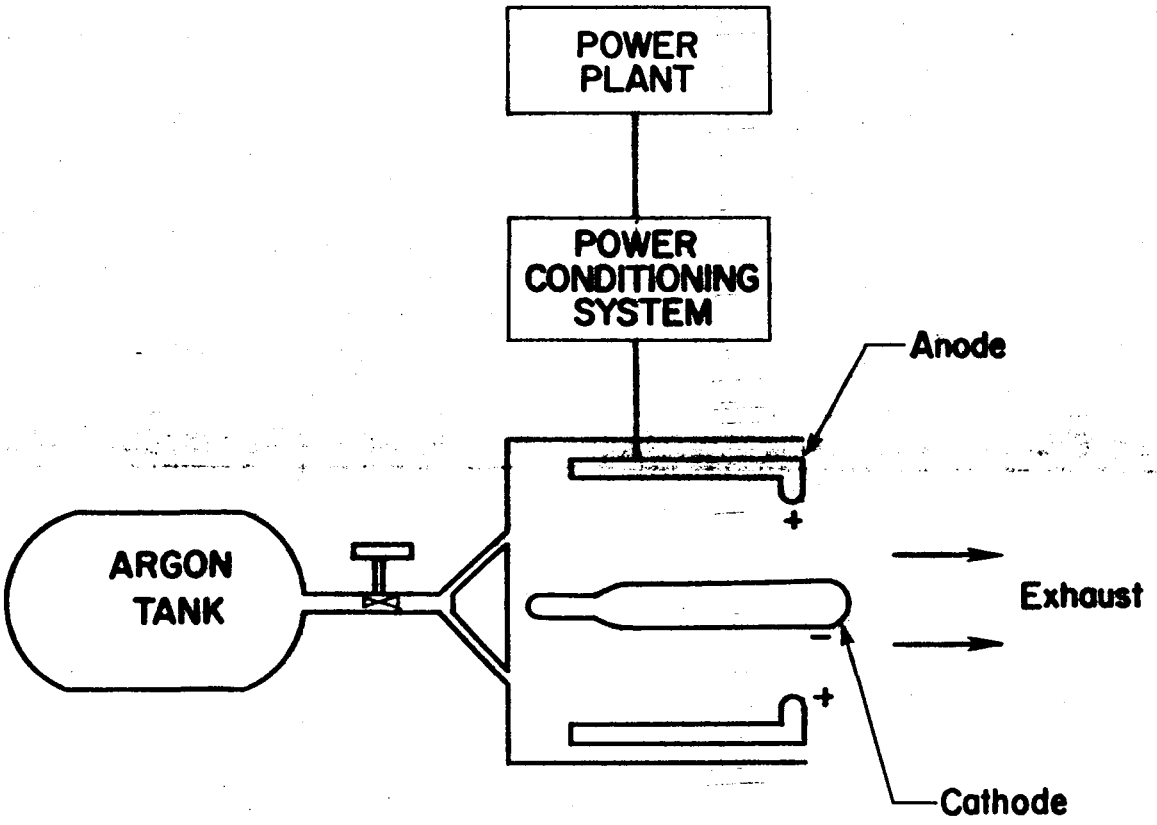

Figure 3. Schematic Diagram of a MPD Thruster.

as heat. The hot recombined gas is expanded through a nozzle to produce thrust. A schematic diagram of a free radical thruster is shown in Fig. 4.

Mercury Electron Bombardment Ion Thruster[27-29]

In these thrusters, neutral mercury atoms are fed to an ion source and the positive ions generated are accelerated by an electrostatic field. The positive ions are formed through ionization in a discharge chamber by electron bombardment where electrons are emitted from an electrically heated cathode filament and are attracted by a surrounding cylindrical anode. The electrons are made to spiral through mercury vapor by applying an axially divergent magnetic field to improve ionization efficiency.

The positive ions are extracted and accelerated by a multiple-aperture dished accelerator screen grid system. The first electrode is maintained at a negative potential with respect to the ion source and the second electrode is kept slightly positive with respect to the first one. After being expelled from the thruster the positive ion beam is neutralized by the addition of an equal number of negative electrons. Fig. 5 shows a schematic drawing of an ion thruster.

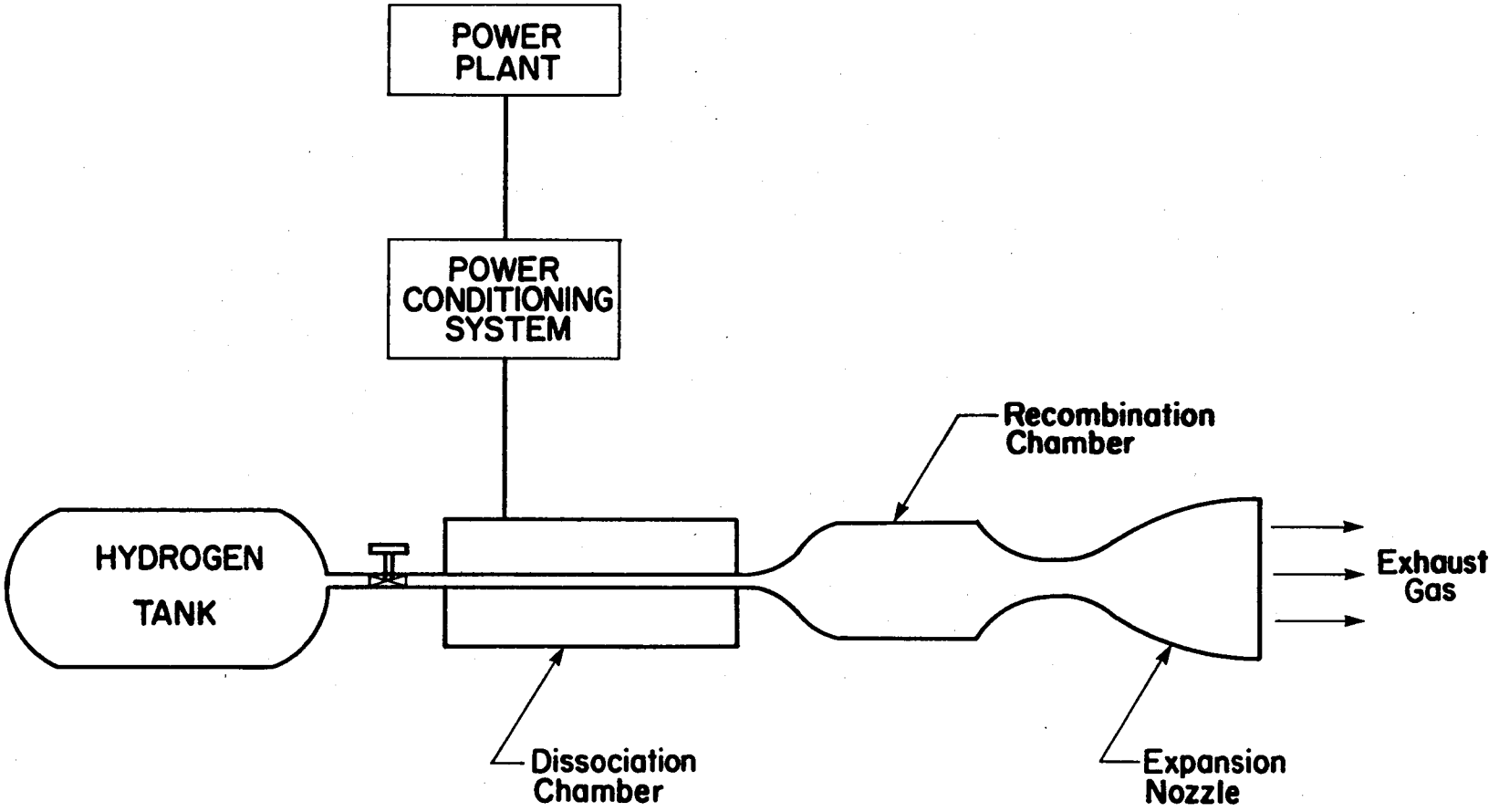

Figure 4. Schematic Diagram of a Hydrogen Free Radical Thruster.

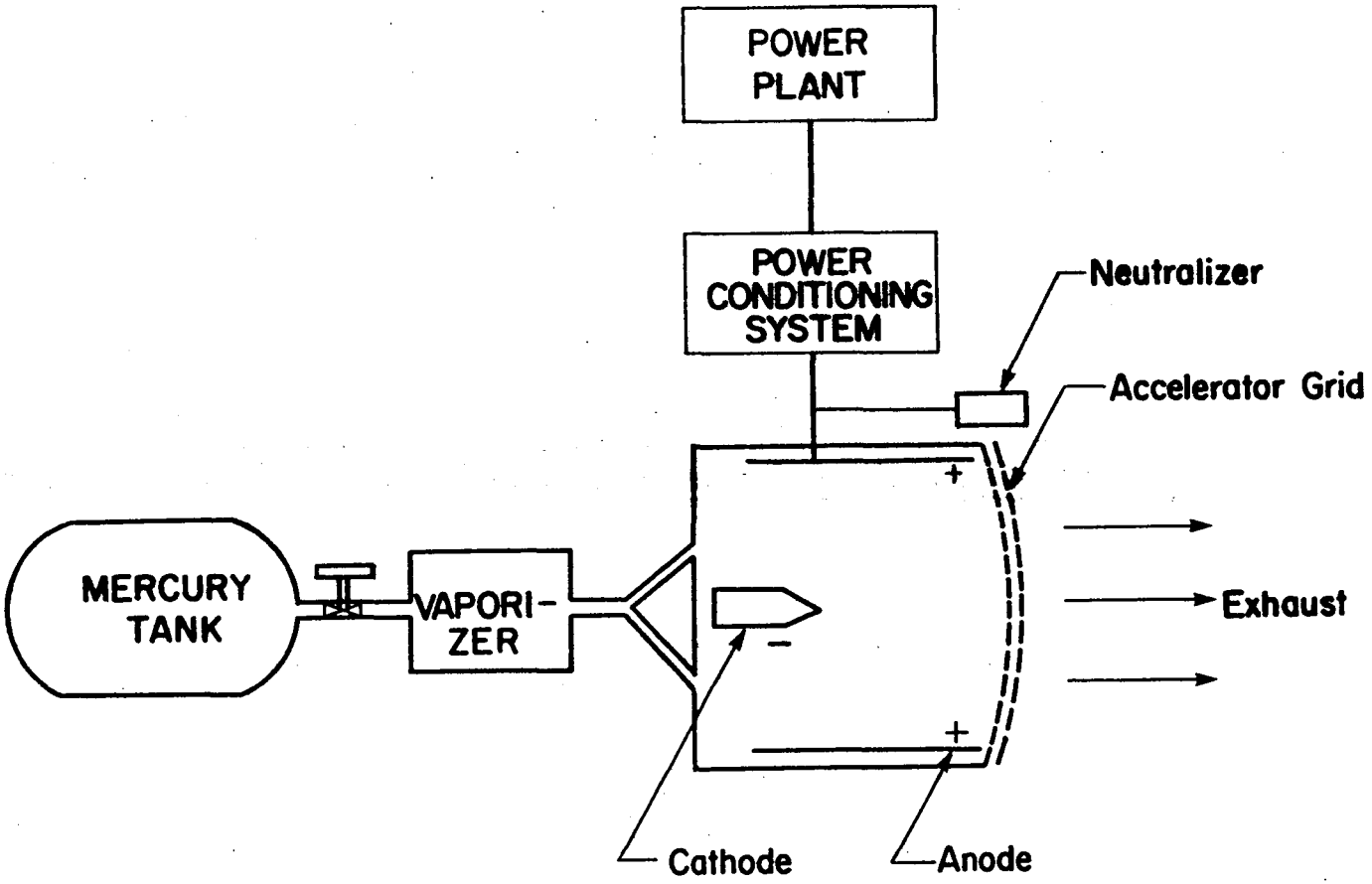

Figure 5. Schematic Diagram of a Mercury Electron Bombardment Ion Engine.

RESULTS

For a comparative evaluation, the electric propulsion systems are characterized by specific impulse, overall efficiency, input power requirement, thurst, power to thrust ratio and thrust to weight ratio. For propulsion systems operating in an impulsive mode, the pertinent characteristics are specific impulse, overall efficiency, input power, average thrust, power to average thrust ratio and average thrust to dry weight ratio. Besides, there are several important physical characteristics such as dry system mass, accelerator length, bore size and current pulse requirement and these are also evaluated in appropriate cases.

Overall efficiency is obtained by dividing the average kinetic power output of the exhaust beam by the required input power from the power plant. The average thrust is calculated by using the equations outlined in the appendices. Dry system mass and dry weight represent the masses and weights of all components except fuel.

The efficiency of the power conditioning system has been assumed to be 0.9 in all cases except ion engine. The power plant specific mass is assumed to be 10 kg/kw. For mass driver and rail gun, the radiator specific mass is assumed to be 10 kg/kw and the power conditioning system mass is assumed to be 5 kg per kilowatt of input power. It is to be noted that these values are quite optimistic. Characteristics of each of the five electric propulsion systems are presented in the following sections.

Mass Driver

For the purpose of this study, we have selected a reference design of a coaxial mass driver reaction engine by O'Neill.[12] In this

design, the diameter of the drive winding is set at 5 cm and that of the bucket is 1.3 cm. The mass of the bucket is 22 gm and it can carry 25,000 amp/cm^2 at superconducting temperature. The peak drive current is 7,580 amp-turns. The frequency of launch is taken to be 5 Hz. The equations and data used to calculate the characteristics of mass driver are presented in Appendix A.

For this mass driver design, projectile mass and specific impulse are used as the variables. The mass of the projectile is varied from 1 gm to 30 gm for two values of specific impulse, 1000 sec and 1500 sec. Mass driver characteristics are determined for several combinations of projectile mass and specific impulse.

Overall efficiency of the mass driver is plotted in Fig. 6 against projectile mass for the two specific impulses. It is observed that the efficiency is quite low for smaller projectile masses. However, it rapidly rises to a high value (greater than 50 percent) and begins to flatten out thereafter. The efficiency is higher when mass drivers are operated at higher specific impulse.

Figures 7 and 8 show the effect of variation of projectile mass on the input power and the average thrust of the mass driver. The input power requirement ranges from a megawatt to tens of megawatts and the average thrust varies from tens of newtons to thousands of newtons. These devices are extremely long (tens of kilometers, Fig. 9) and hence, very massive (Fig. 10).

The power to average thrust ratio is presented in Fig. 11. This ratio is rather high at low projectile masses and approaches an asymptotic value (~9 kw/N at I_{sp} = 1500 sec and ~6 kw/N at I_{sp} = 1000 sec) as

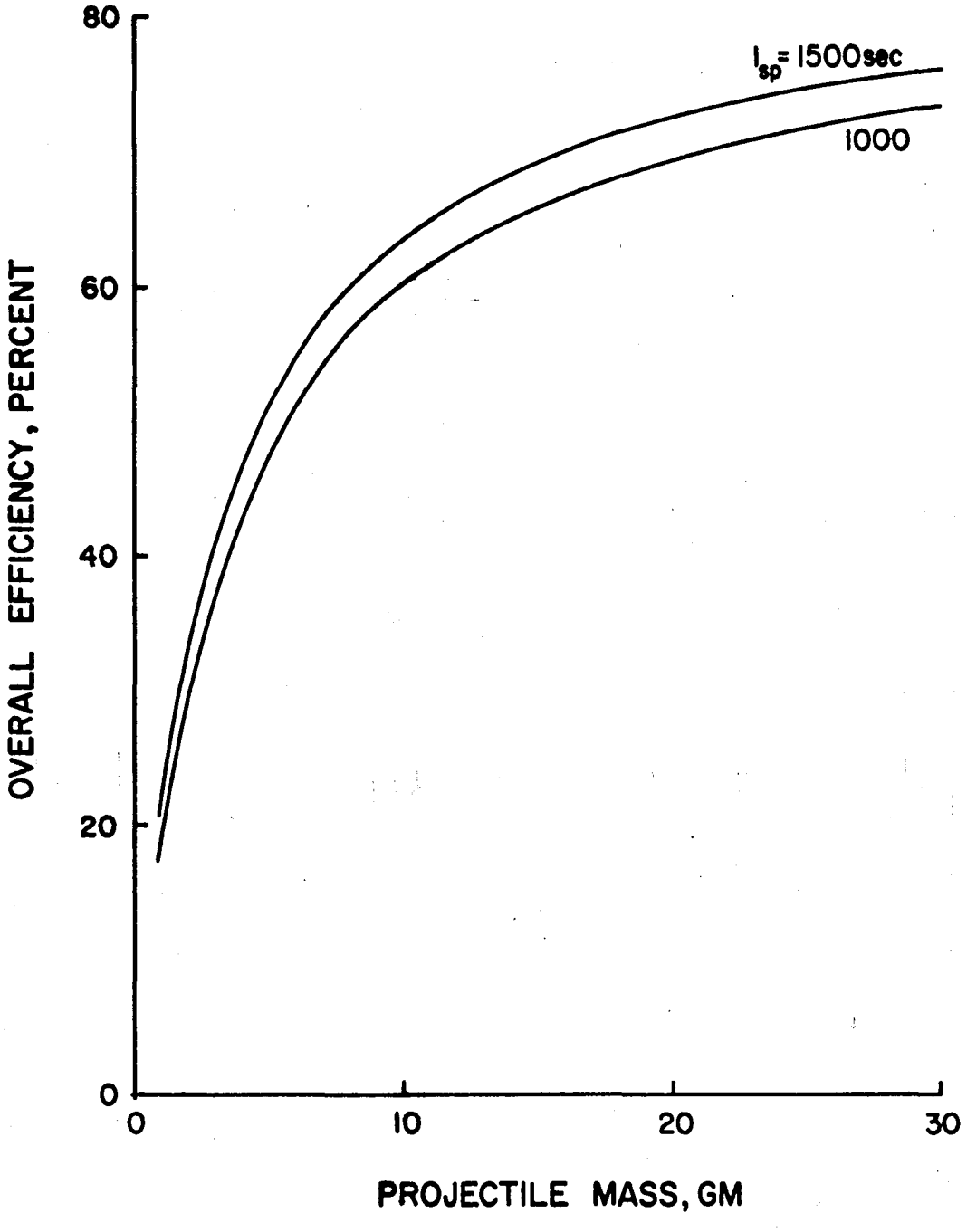

Figure 6. Overall Efficiency of Mass Driver Versus Projectile Mass for Specific Impulses of 1000 and 1500 sec.

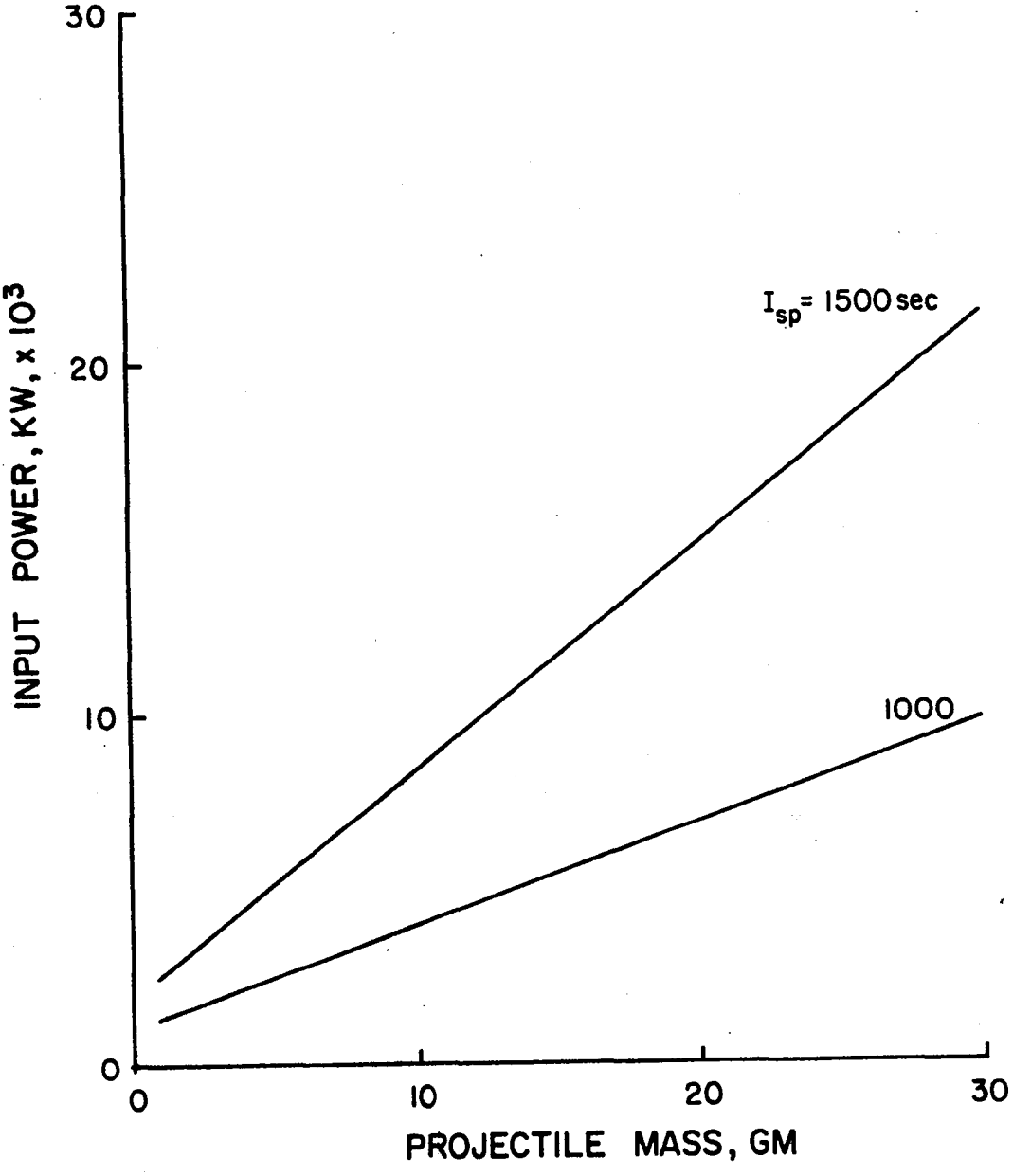

Figure 7. Effect of Projectile Mass on Input Power of Mass Driver for Specific Impulses of 1000 and 1500 sec.

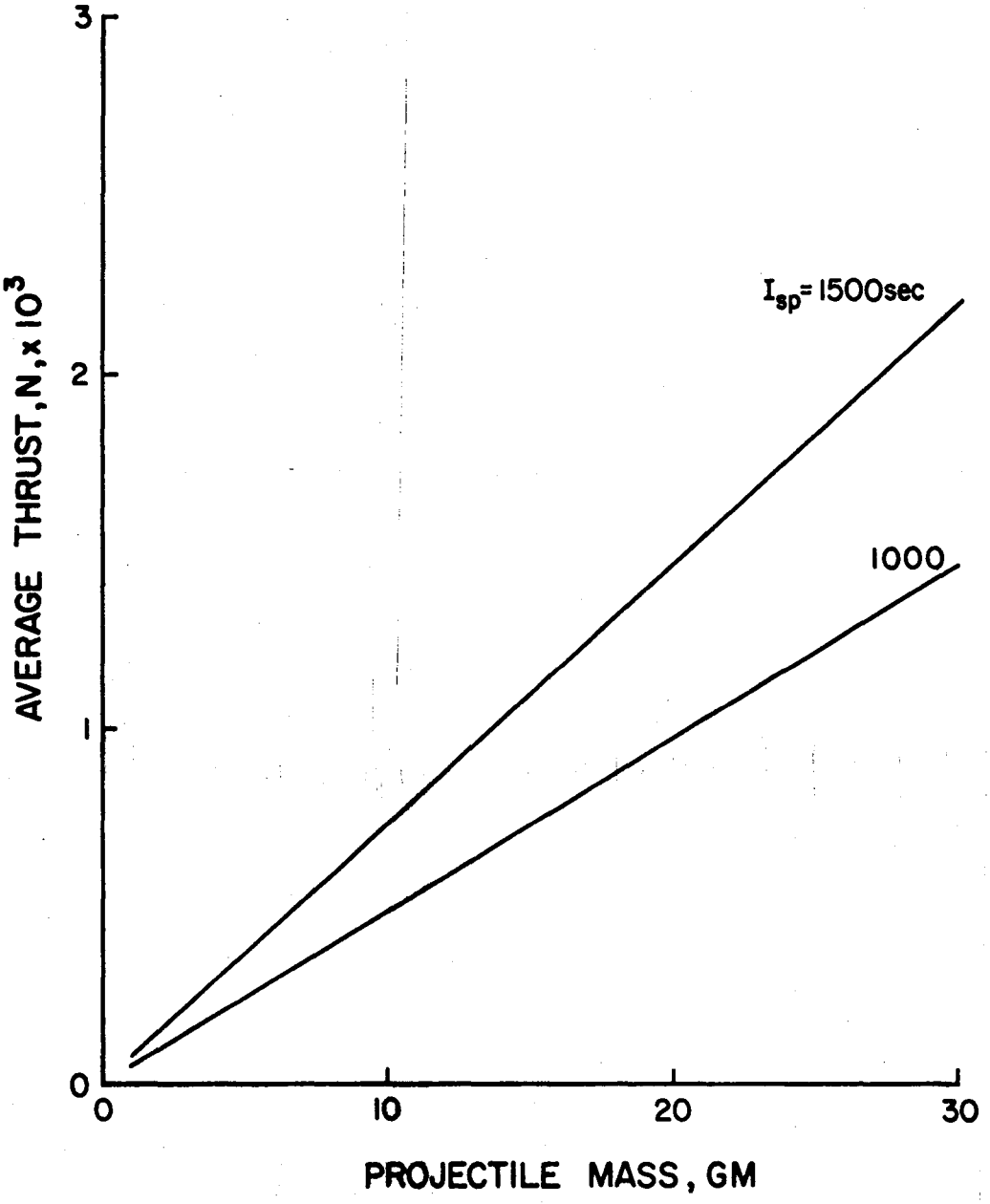

Figure 8. Average Thrust of Mass Driver Versus Projectile Mass for Specific Impulses of 1000 and 1500 sec.

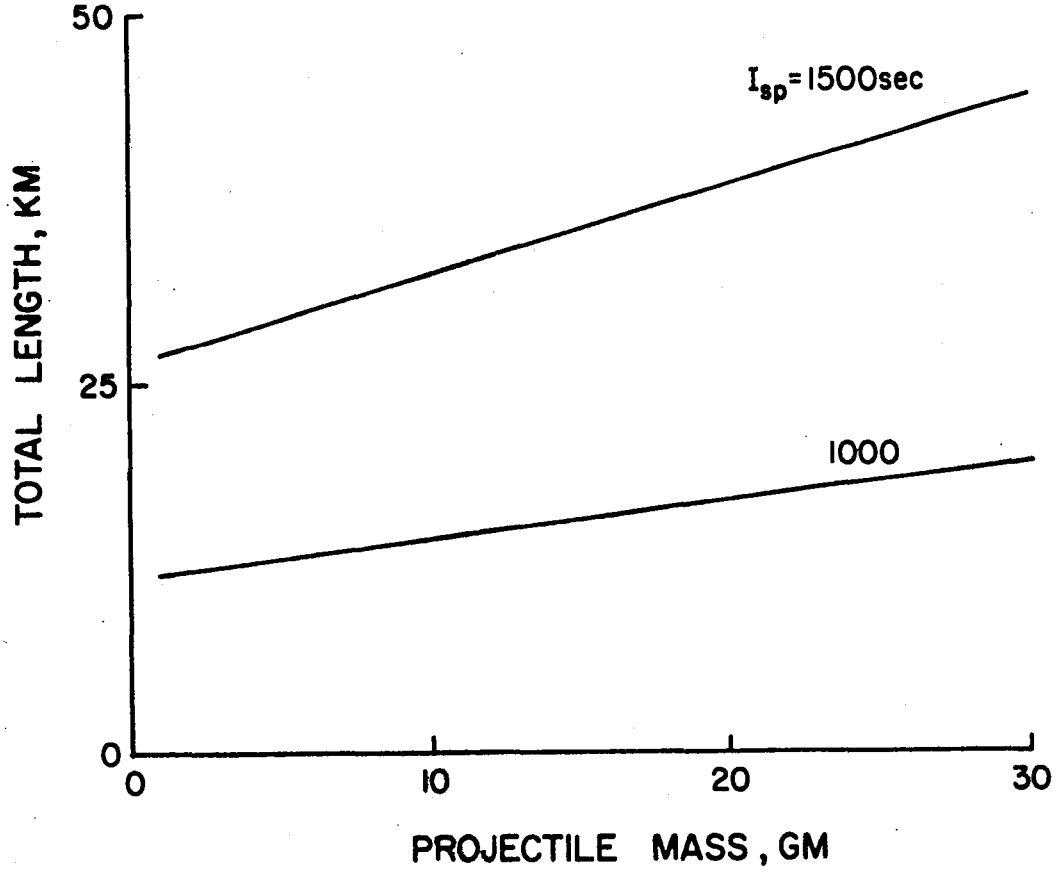

Figure 9. Effect of Projectile Mass on Total Length of Mass Driver for Specific Impulses of 1000 and 1500 sec.

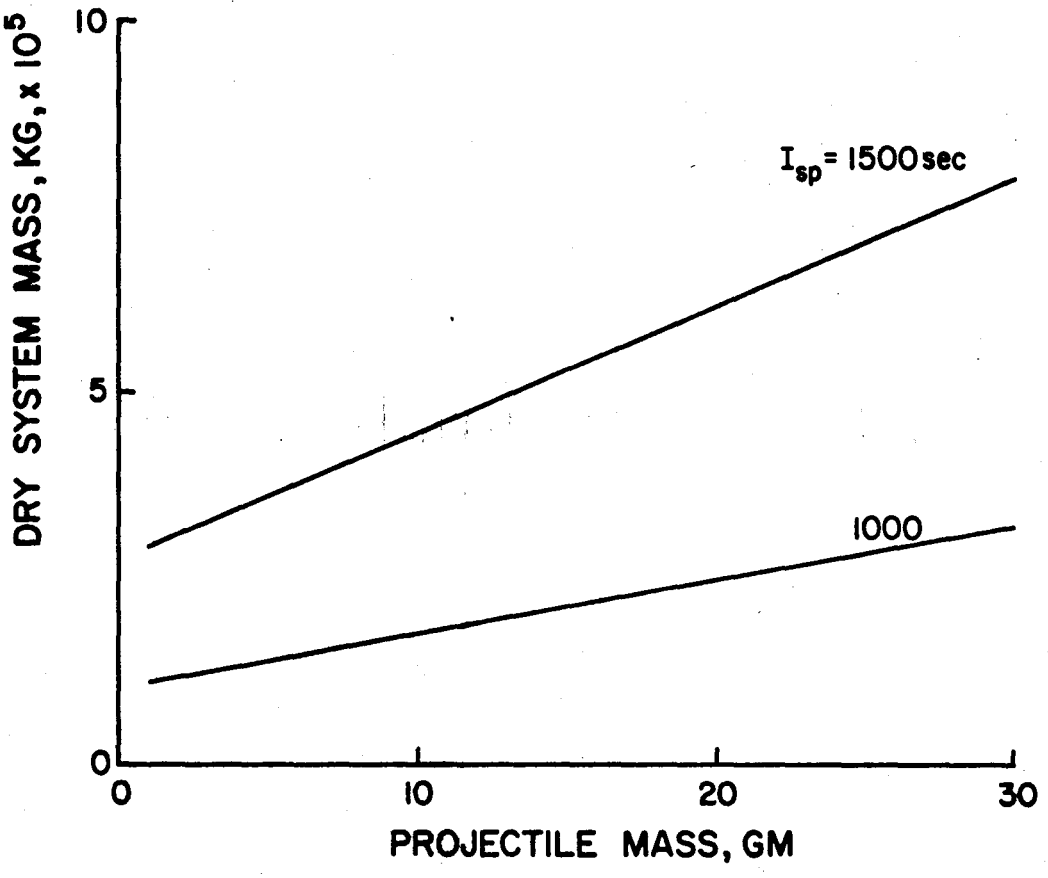

Figure 10. Effect of Projectile Mass on Dry System Mass of Mass Driver for Specific Impulses of 1000 and 1500 sec.

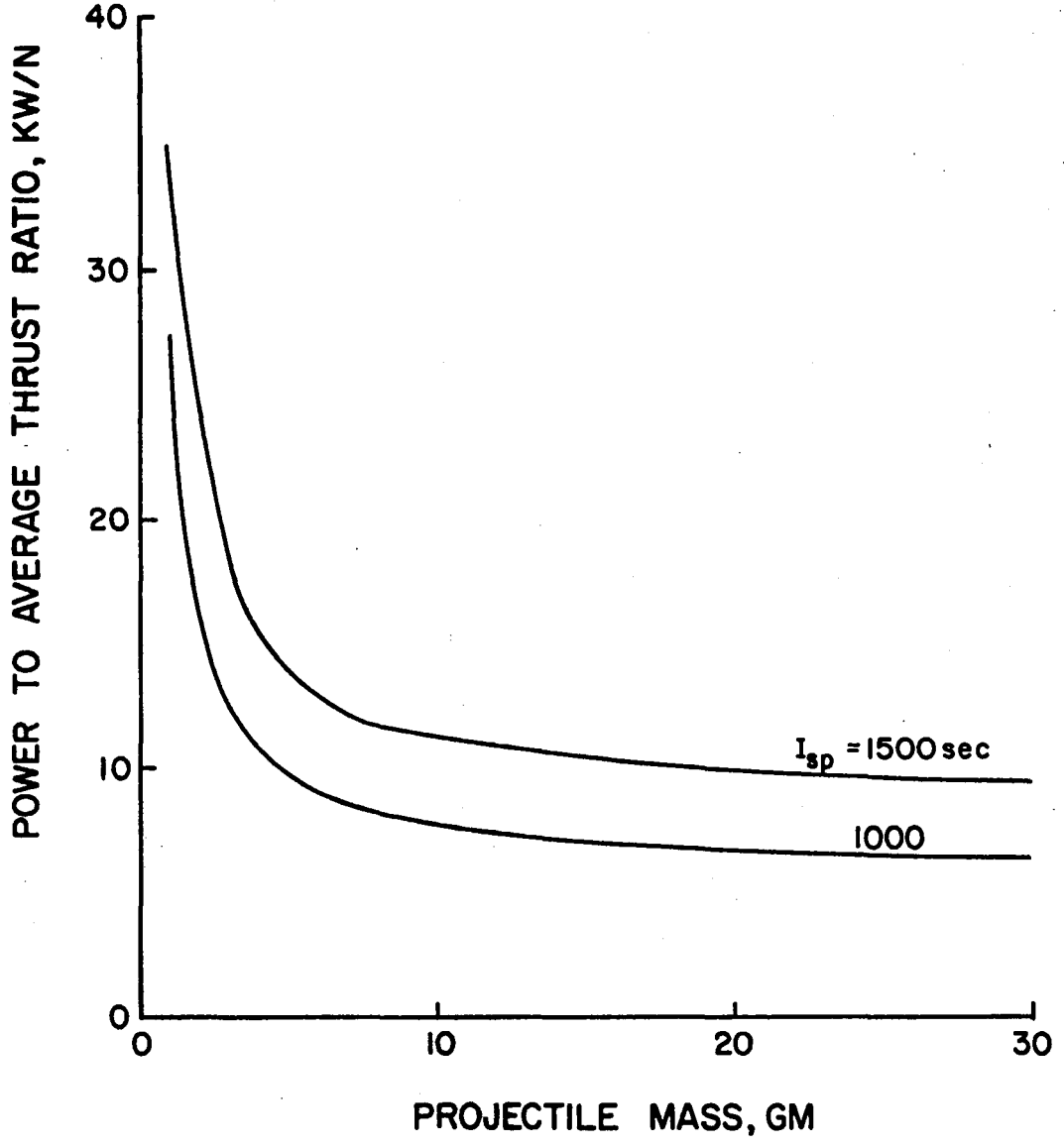

Figure 11. Power to Average Thrust Ratio of Mass Driver Versus Projectile Mass for Specific Impulses of 1000 and 1500 sec.

the mass of the projectile is increased. Figure 12 shows the average thrust to dry weight ratio of the mass driver. For a fixed specific impulse, it increases with increase in projectile mass. This ratio decreases when specific impulse is increased.

Rail Gun Thruster

The characteristics of rail gun thrusters have been evaluated by using the correlations developed by Bauer et al.[19] The accelerator is assumed to have a square bore and the projectile thickness is assumed to be half of the bore width. To withstand high stresses due to rapid acceleration, the projectile is assumed to be made of a composite of resin and graphite fiber having a density of 2,200 kg/m^3. The launching frequency is taken to be 5 Hz. The equations used in calculating the rail gun characteristics are provided in Appendix B.

Projectile mass and specific impulse are used as the variables in rail gun calculations. The mass of the projectile is varied from 0.1 gm to 1.0 gm for specific impulses of 1000, 1500 and 2000 sec. Characteristics of rail guns are evaluated for several combinations of projectile mass and specific impulse.

Figure 13 shows the overall efficiency of the rail gun against projectile mass for the three specific impulses. It can be seen that the efficiency is rather low; the upper limit is close to 34 percent. At a fixed specific impulse, the efficiency increases with the increase of projectile mass. However, the efficiency progressively decreases as the specific impulse is increased.

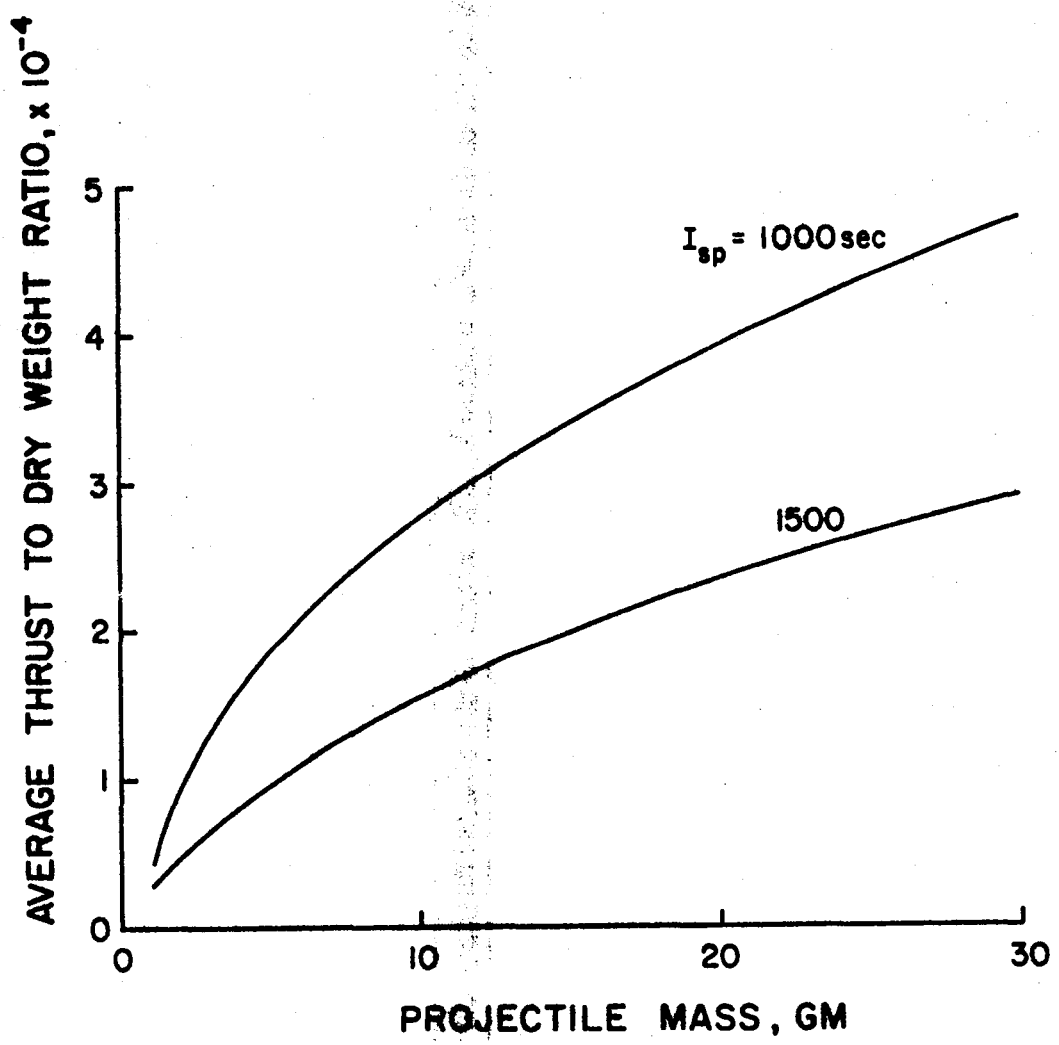

Figure 12. Average Thrust to Dry Weight Ratio of Mass Driver Versus Projectile Mass for Specific Impulses of 1000 and 1500 sec.

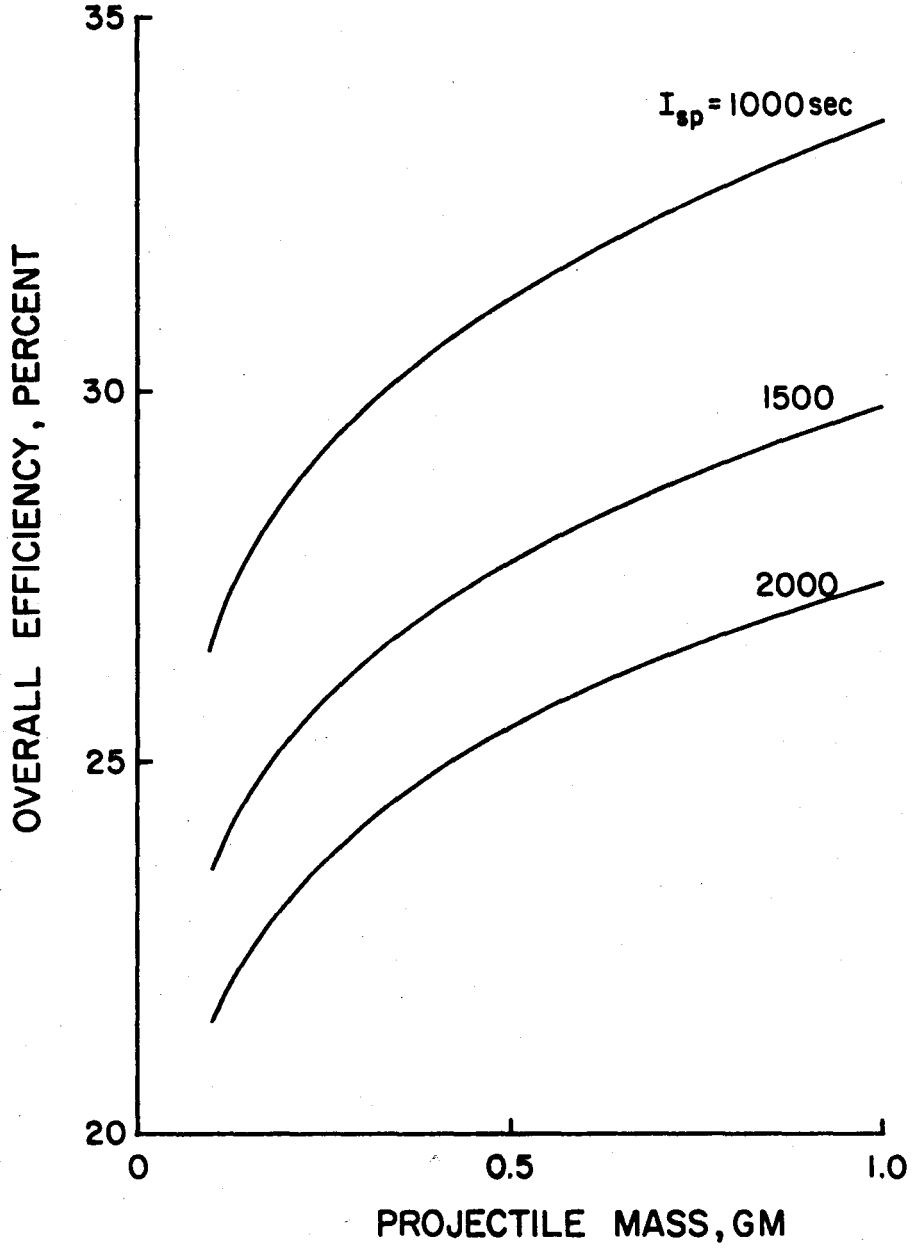

Figure 13. Effect of Projectile Mass on Overall Efficiency of Rail Gun for Specific Impulses of 1000, 1500 and 2000 sec.

The effect of variation of projectile mass on the input power and average thrust of the rail gun is seen in Fig. 14 and Fig. 15 respectively. At low specific impulse and small projectile mass the input power requirement is hundreds of kilowatts and the average thrust is tens of newtons. For gram size projectiles at higher specific impulse, the input power requirement quickly climbs to the megowatt level and the average thrust increases to hundreds of newtons. To achieve higher efficiency, rail guns should be operated at a low specific impulse and a high average thrust (hence, a high input power).

The length of the rail gun varies from tens to hundreds of meters to provide a specific impulse of 1000 sec or more (Fig. 16). Figure 17 indicates the required bore size and it is clear that masses less than 0.1 gm can not be launched from a practical point of view as the bore width has to be less than 4 mm for a 20 m long accelerator. Current pulses required in rail guns vary from 35 KA for launching a mass of 0.1 gm to 75 KA for launching a mass of 1.0 gm (Fig. 18). For a given projectile mass, changing specific impulse has no significant effect on the length and bore size of the accelerator and the current pulse needed. The dry system mass of the rail gun thruster is presented in Fig. 19.

Due to low efficiency of the rail gun, the power to average thrust ratio of this device is rather high, particularly at specific impulses of 1500 and 2000 sec (Fig. 20). For a given specific impulse, this ratio decreases slowly as the projectile mass is increased. The average thrust to dry weight ratio is presented in Fig. 21. For a given specific impulse, it increases slowly with increase in projectile mass. This ratio decreases when specific impulse is increased.

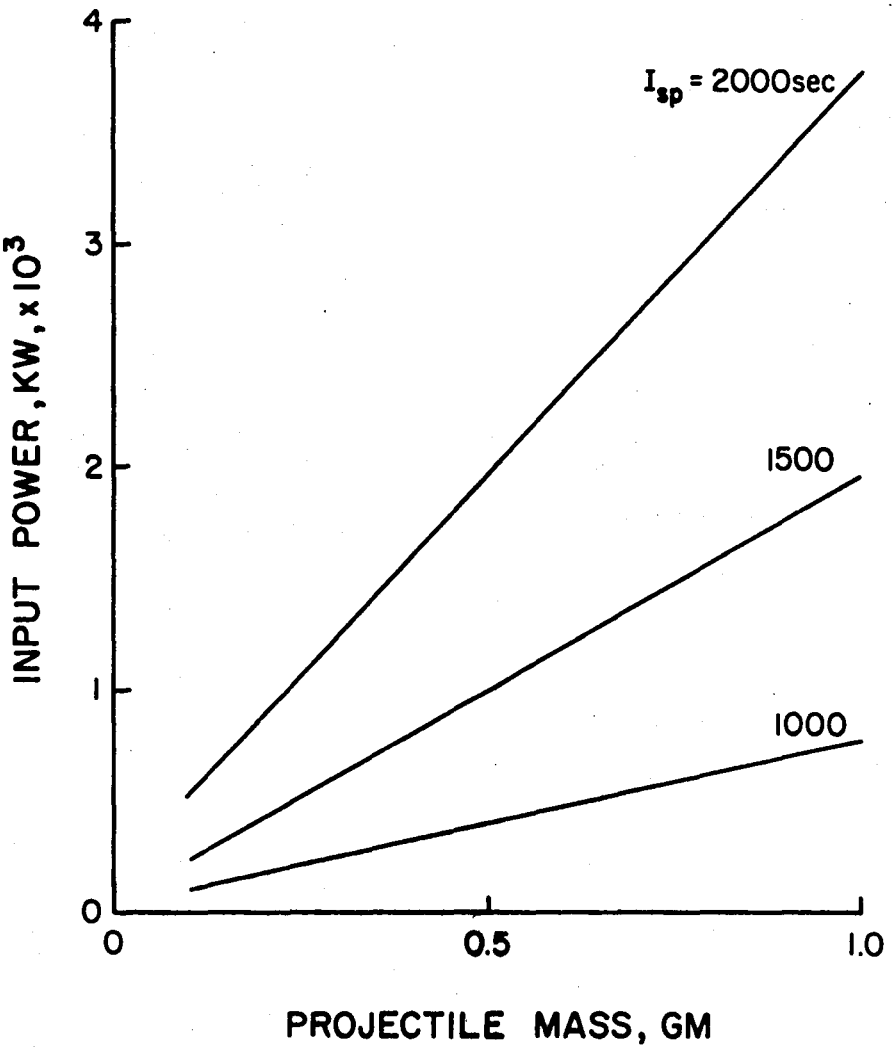

Figure 14. Effect of Projectile Mass on Input Power of Rail Gun for Specific Impulses of 1000, 1500 and 2000 sec.

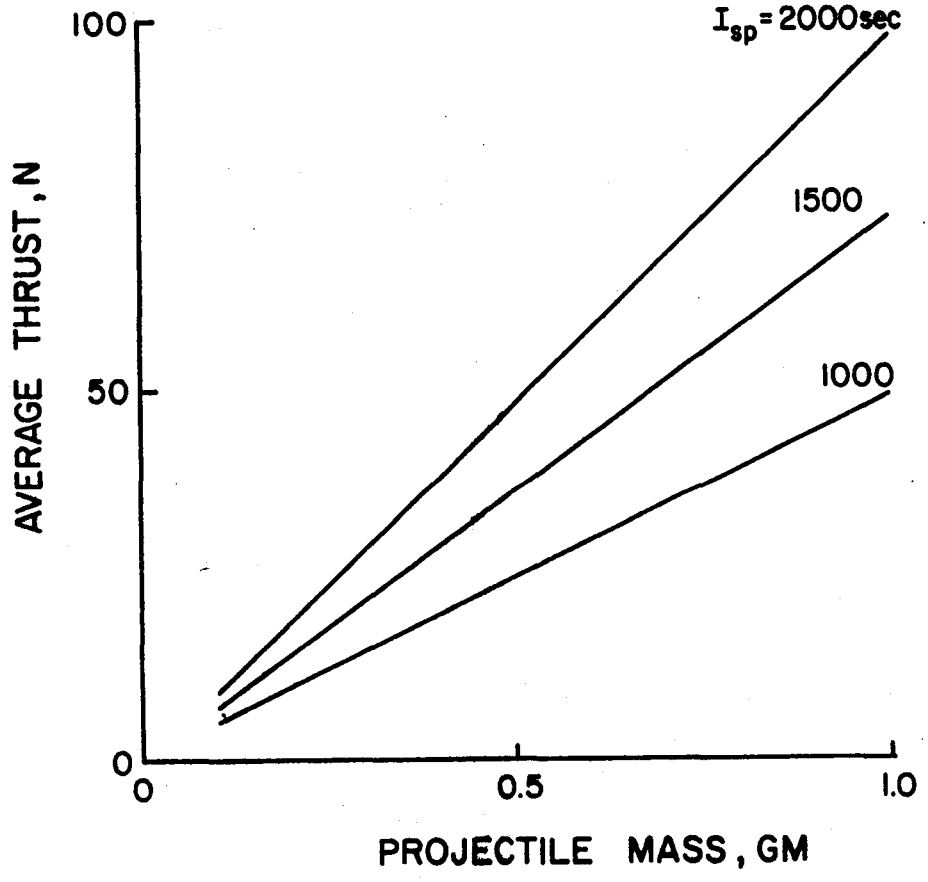

Figure 15. Average Thrust of Rail Gun Versus Projectile Mass for Specific Impulses of 1000, 1500 and 2000 sec.

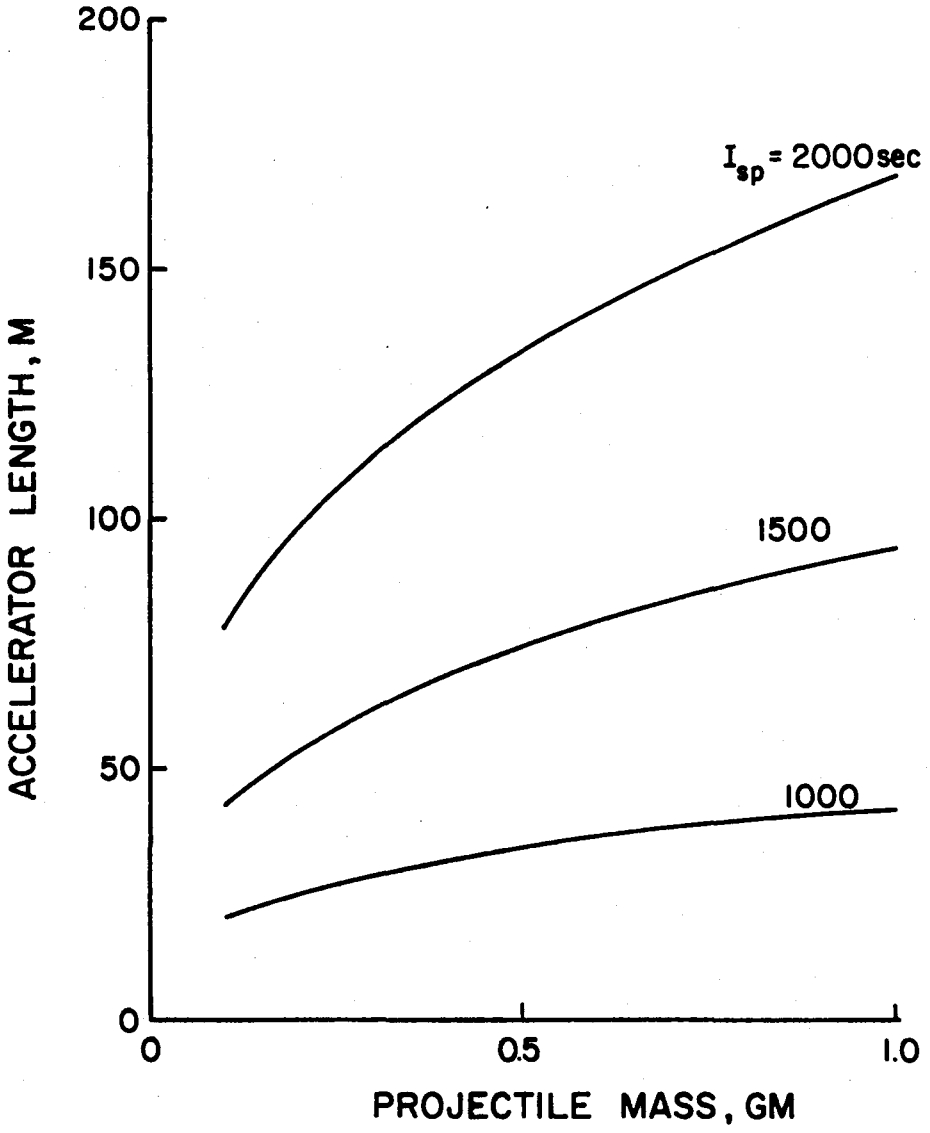

Figure 16. Effect of Projectile Mass on Length of Rail Gun for Specific Impulses of 1000, 1500 and 2000 sec.

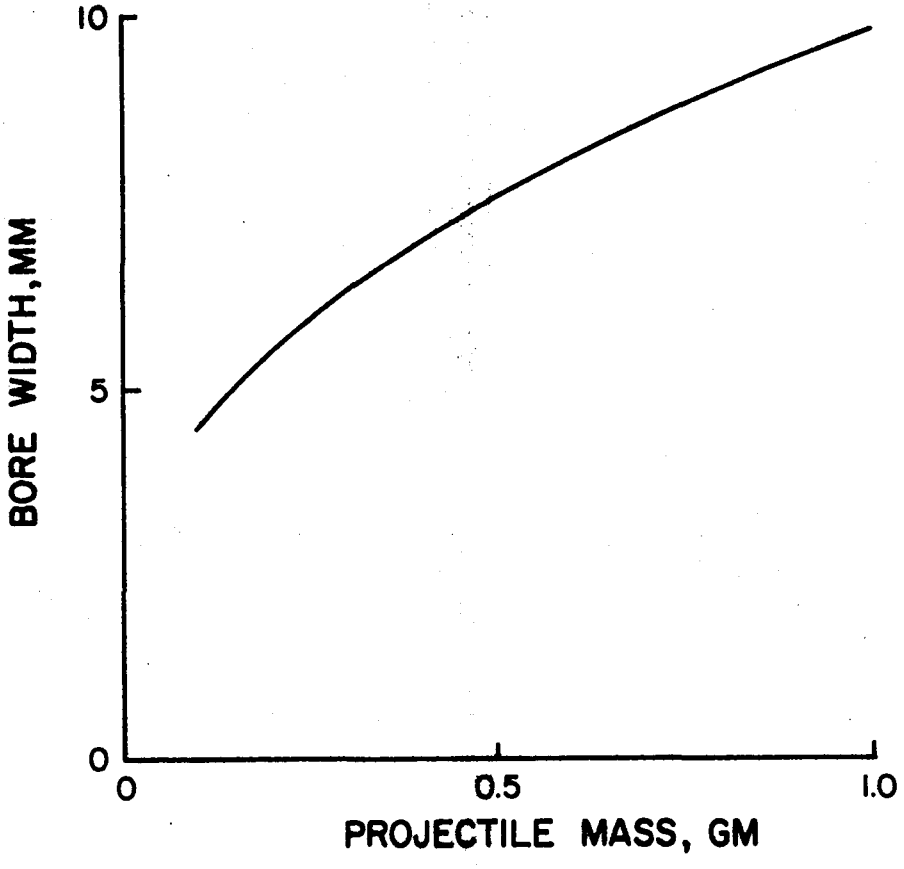

Figure 17. Effect of Projectile Mass on Bore Width of Rail Gun.

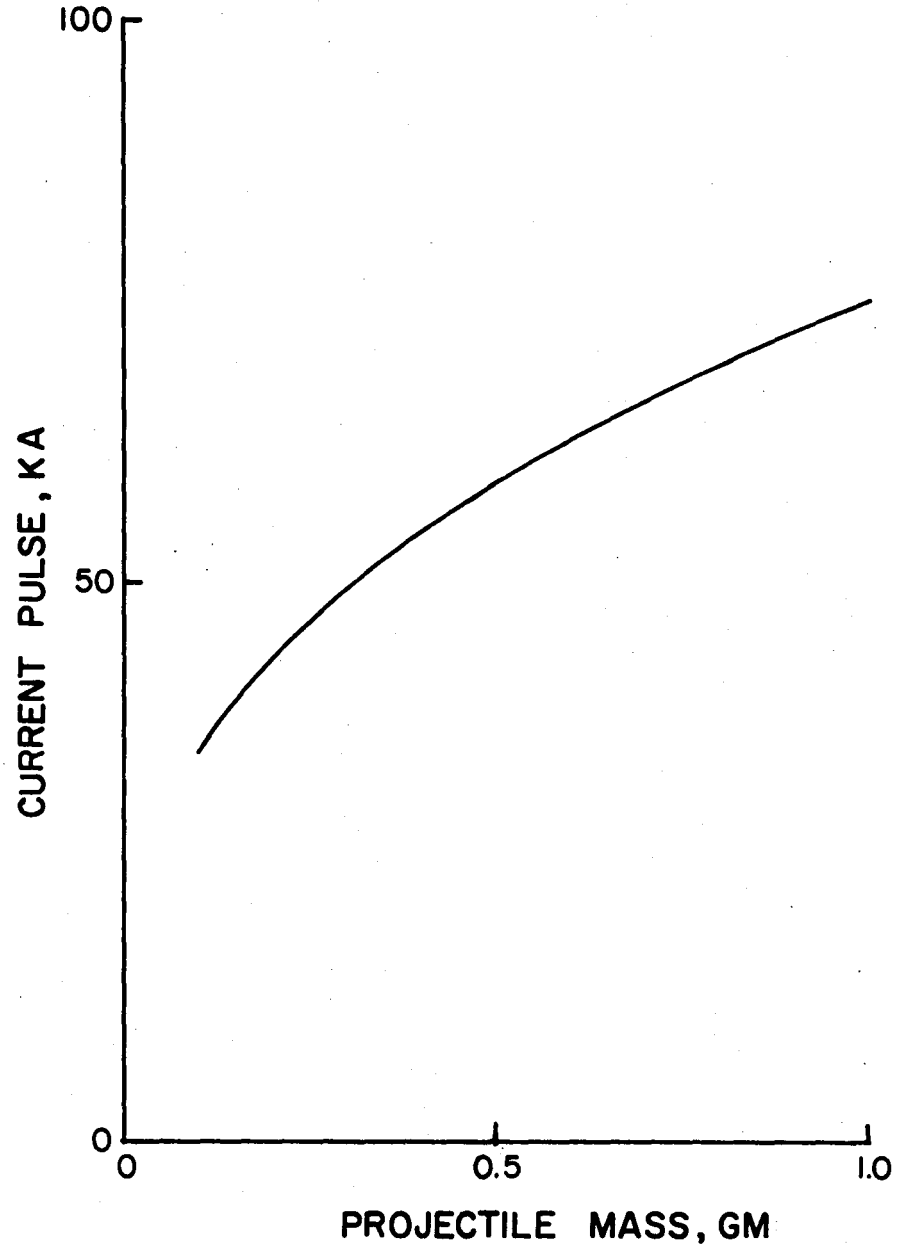

Figure 18. Effect of Projectile Mass on Current Pulse Requirement of Rail Gun.

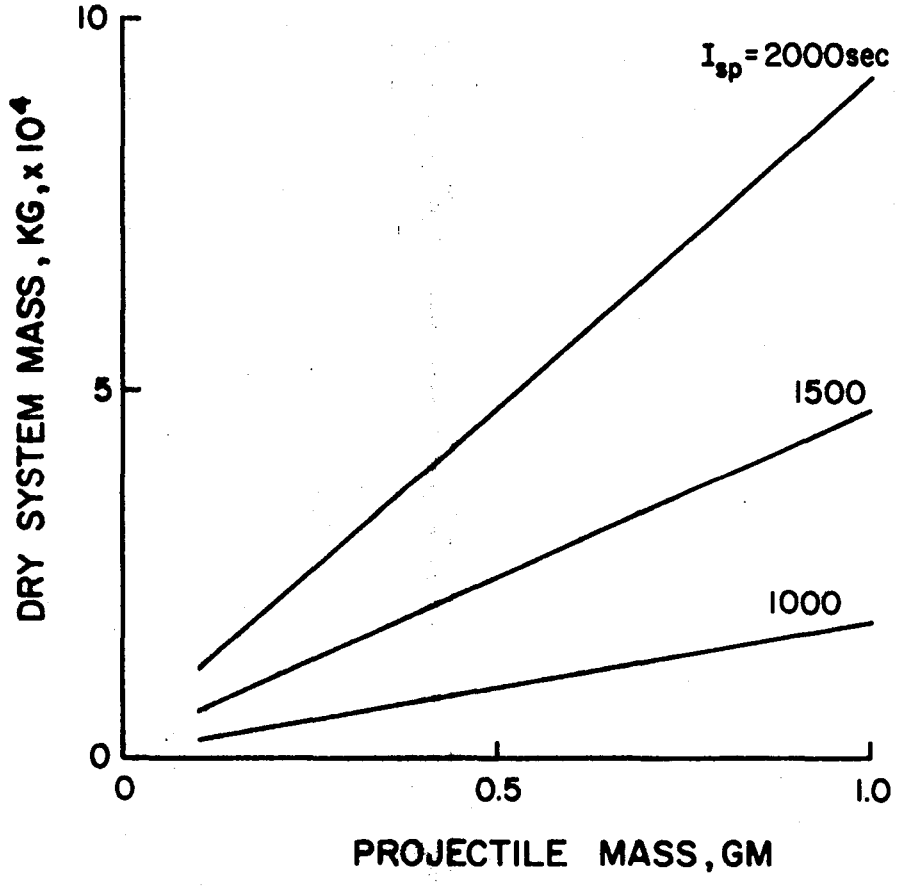

Figure 19. Dry System Mass of Rail Gun Versus Projectile Mass for Specific Impulses of 1000, 1500 and 2000 sec.

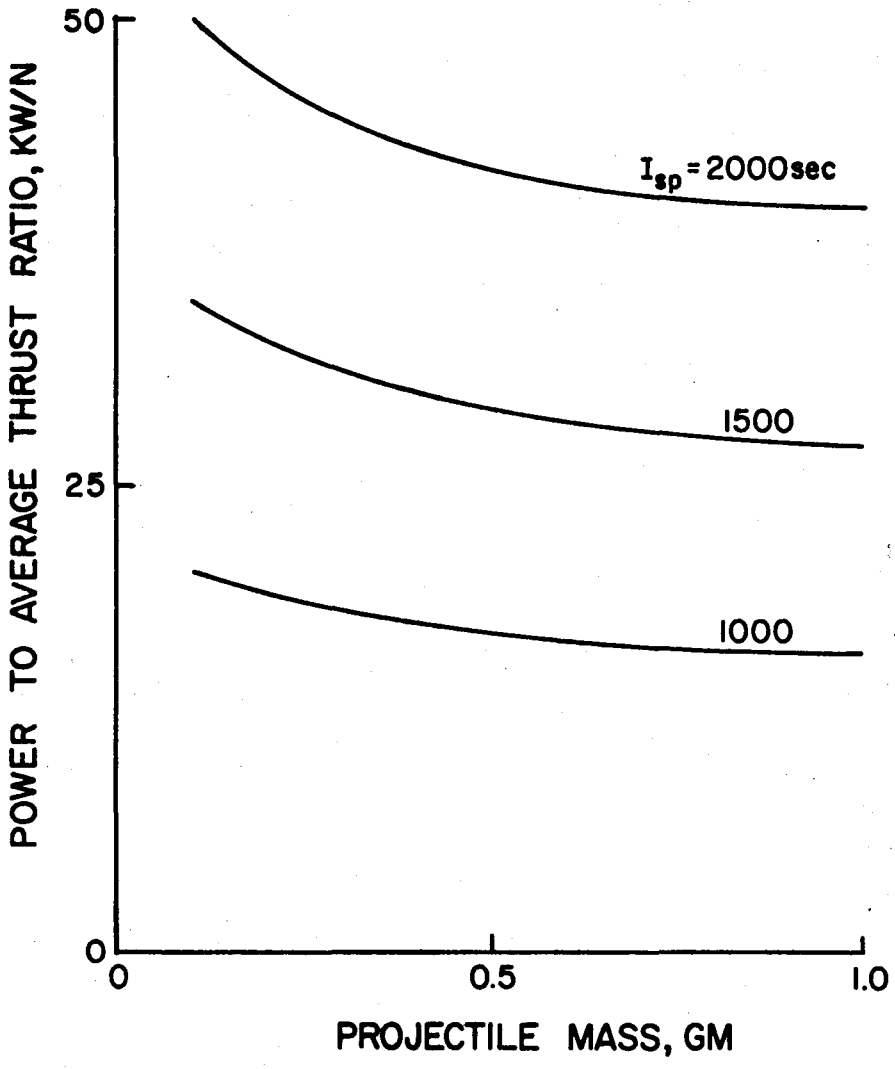

Figure 20. Effect of Projectile Mass on Power to Average Thrust Ratio of Rail Gun for Specific Impulses of 1000, 1500 and 2000 sec.

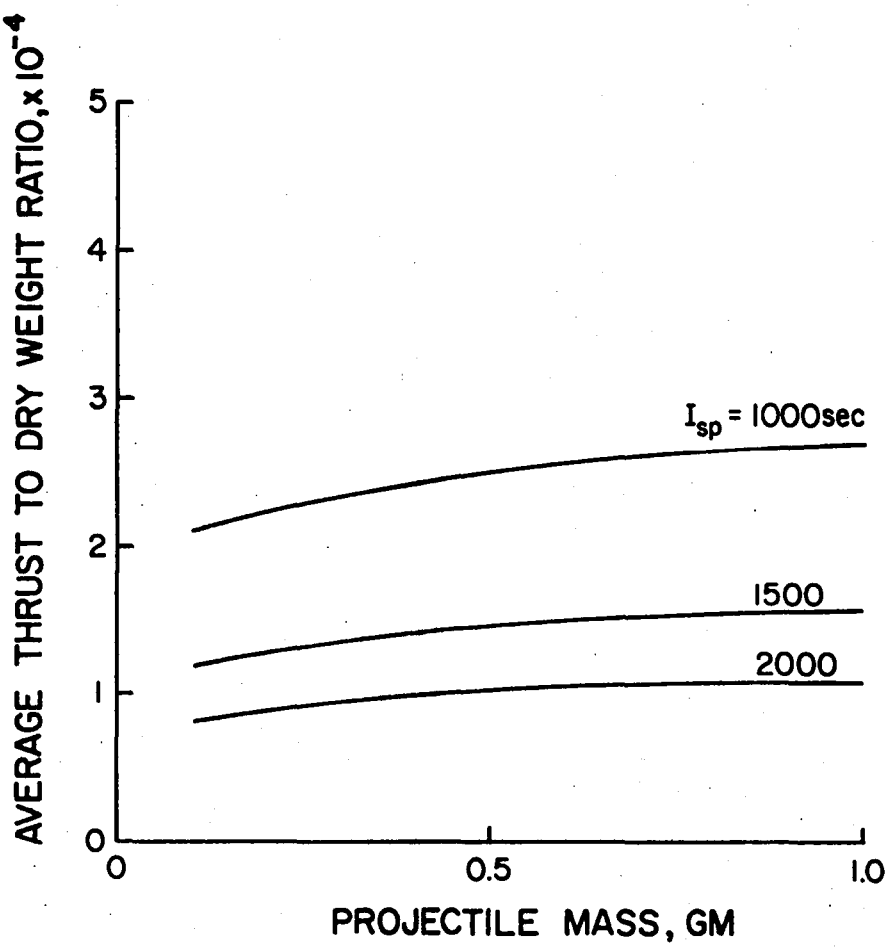

Figure 21. Average Thrust to Dry Weight Ratio of Rail Gun Versus Projectile Mass for Specific Impulses of 1000, 1500 and 2000 sec.

MPD Thruster

The MPD thruster characteristics are evaluated by using the experimental data obtained from an argon self-field MPD device.[8] Current impulses in the range of 10 to 20 KA and average gas flows in the range of 1.5 to 9.0 gm/sec have been used in these experiments to provide specific impulses from 200 to 2200 sec. The thruster terminal voltage ranged from 40 to 155 volts. The data used represent the operating range before the onset of the voltage fluctuations. We have assumed that the current discharge lasts for 1 msec and the charging time is 9 msec. The cycle time is thus 10 msec. The equations used to determine the MPD thruster characteristics are presented in Appendix C.

Overall efficiency of MPD thruster is plotted against specific impulse in Fig. 22. These thrusters are currently characterized by low efficiencies. Input power and average thrust are presented in Fig. 23 and Fig. 24 respectively. The input power requirement is several hundreds of kilowatts and the average thrust is a few newtons. Due to low efficiencies, the power to thrust ratios of these devices are rather high, particularly if they are to be operated at higher specific impulses (in excess of 40 kw/N, Fig. 25). Due to insufficient design information about the thrust chamber, MPD thruster system mass could not be determined.

Free Radical Thruster

To obtain free radical thruster characteristics, the molar ratio of H_2 and H in the recombination chamber is varied from 0:1 to 10:1. It is assumed that 50 percent of the energy released in recombination is available as the kinetic energy of the exhaust beam. Due to lack of

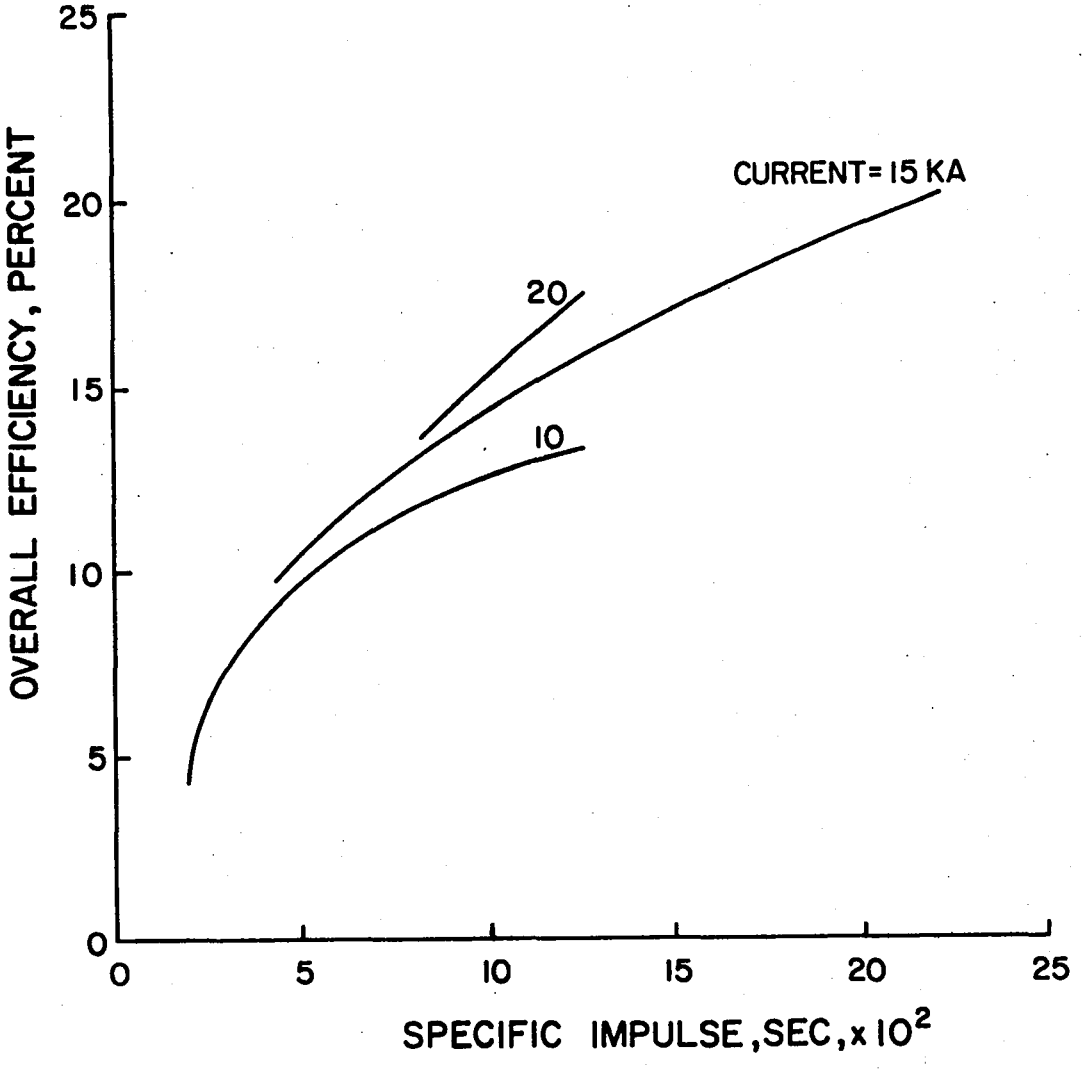

Figure 22. Overall Efficiency of MPD Thruster Versus Specific Impulse for Current Pulses of 10, 15 and 20 KA.

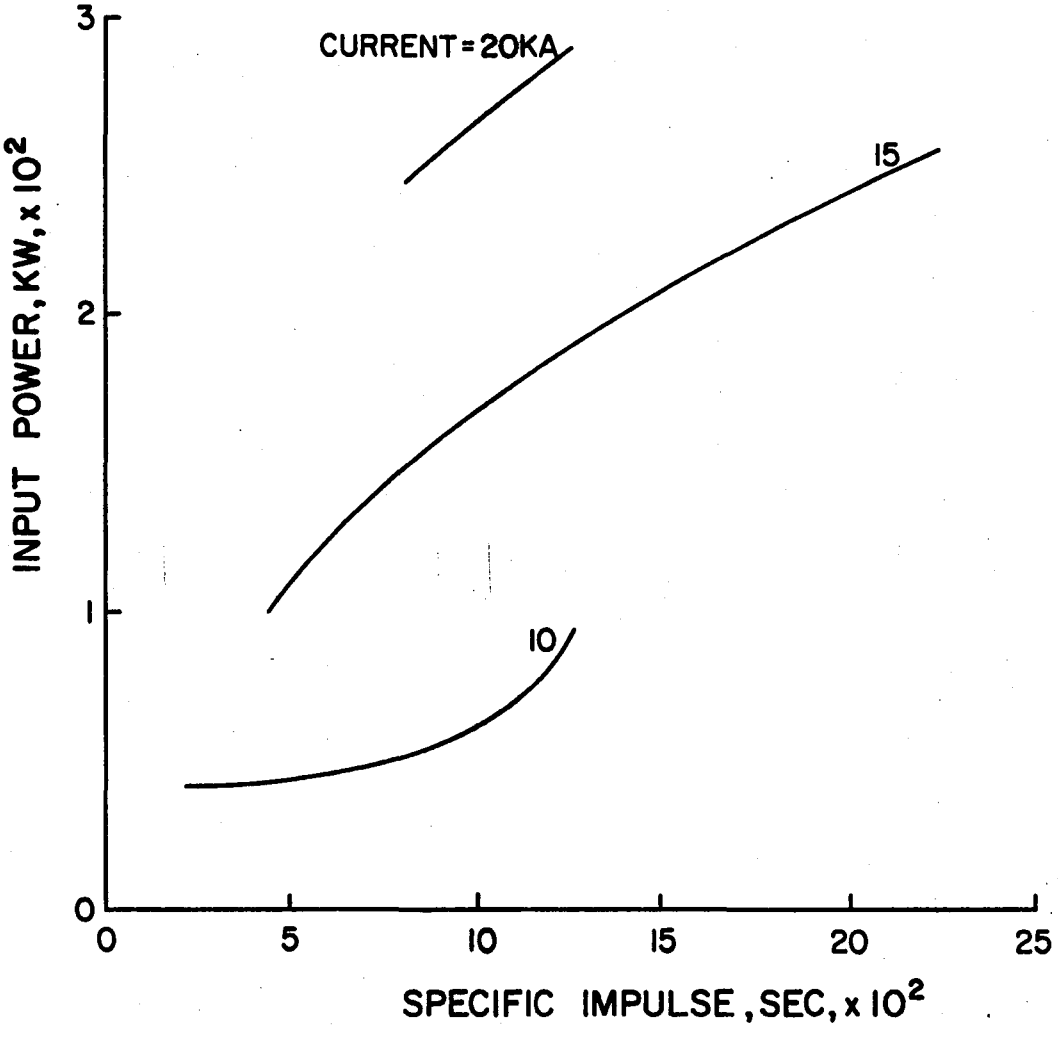

Figure 23. Input Power of MPD Thruster Versus Specific Impulse for Current Pulses of 10, 15 and 20 KA.

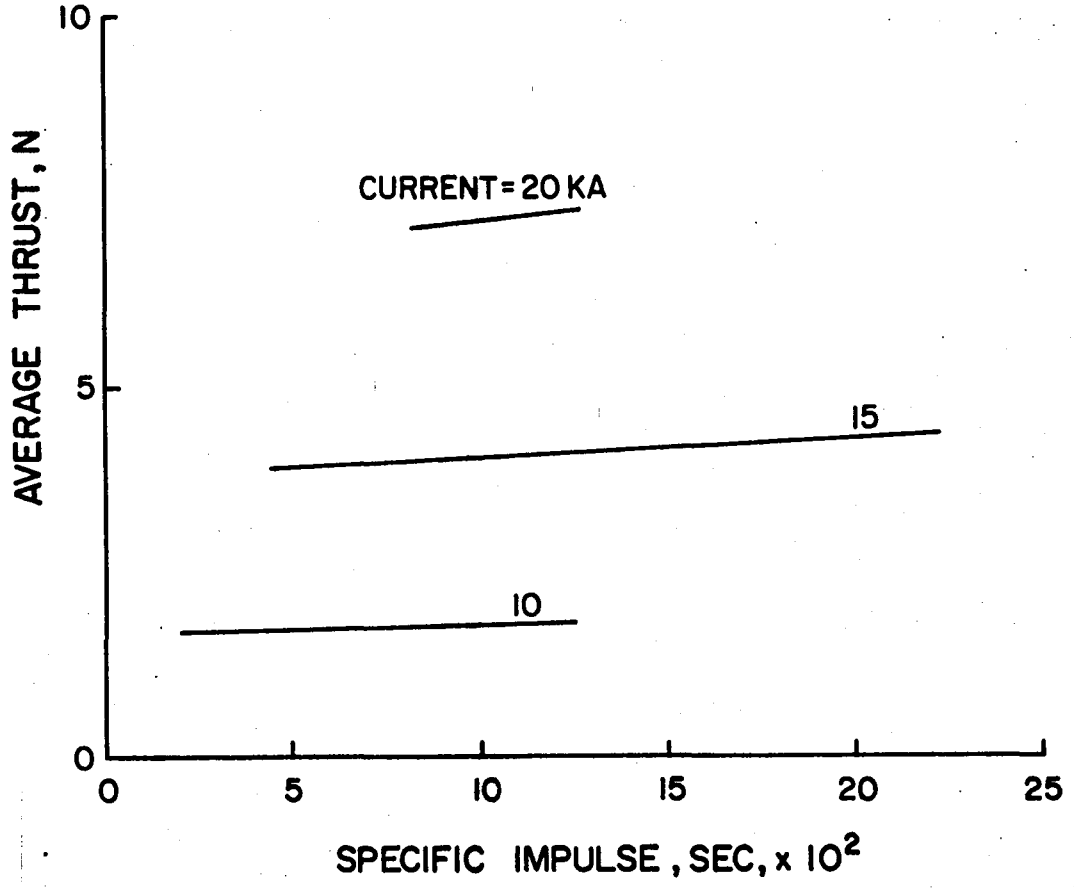

Figure 24. Average Thrust of MPD Thruster Versus Specific Impulse for Current Pulses of 10, 15 and 20 KA.

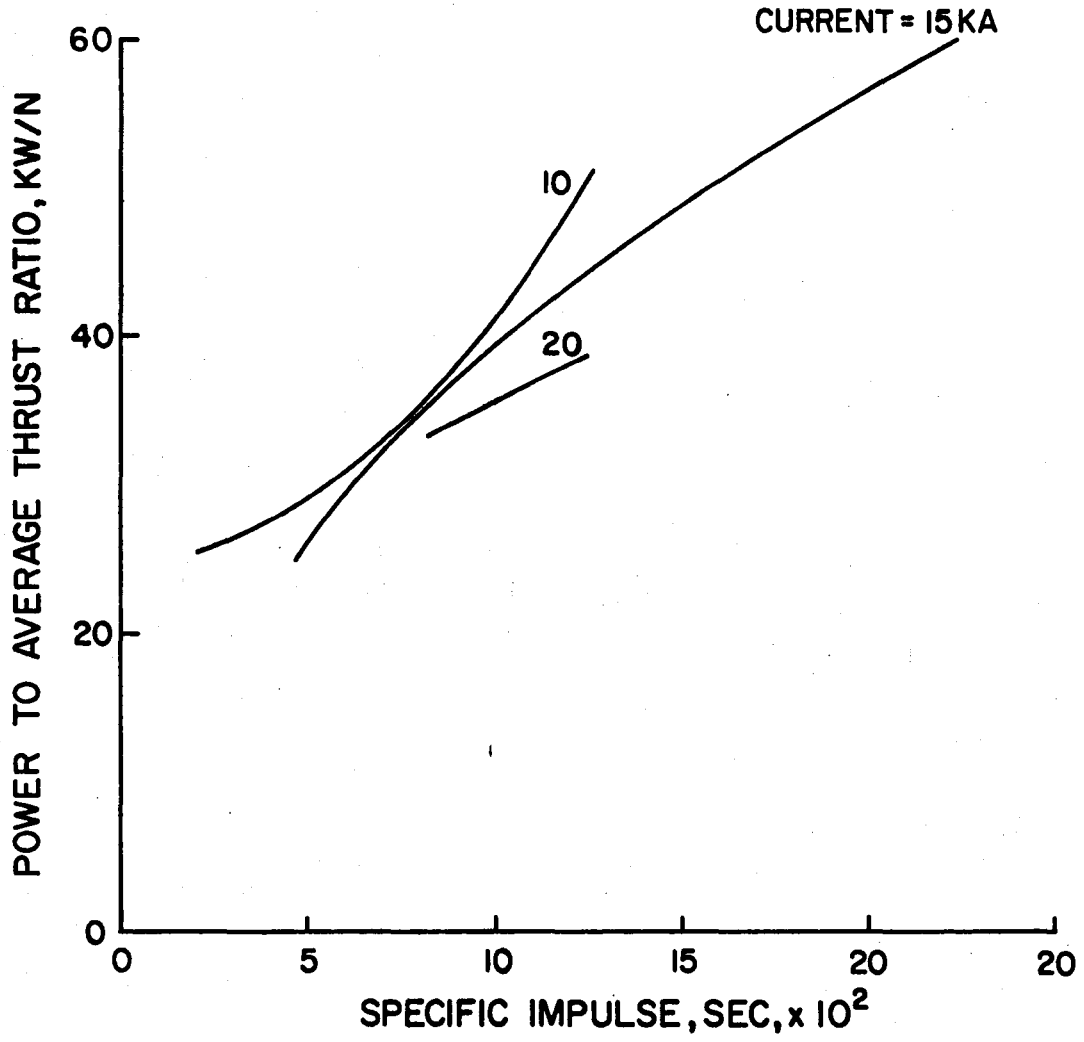

Figure 25. Effect of Specific Impulse on Power to Average Thrust Ratio of MPD Thruster for Current Pulses of 10, 15 and 20 KA.

sufficient experimental or design information about the plasma cavity, we have assumed the microwave energy conversion efficiency to produce the desired H_2:H molar ratios as 0.3 and 0.6 to reflect two possible designs. The H_2 flow rate is assumed to be 1 gm/sec. The relevant equations are listed in Appendix D.

Under the conditions mentioned above, the specific impulse of hydrogen free radical thruster varies from 325 sec (for H_2:H = 10:1) to 1500 sec (for H_2:H = 0:1) as shown in Fig. 26. The thrust produced is tens of newtons (Fig. 27) and the input power ranges from tens to hundreds of kilowatts (Fig. 28). The power to thrust ratio is high for low H_2:H molar ratios (Fig. 29) which implies higher specific impulses. Due to insufficient information about the design of dissociation and recombination chambers, mass of the free radical thruster could not be determined.

Mercury Electron Bombardment Ion Engine

The characteristics of a 50 cm dia mercury electron bombardment ion engine are evaluated for specific impulses ranging from 2000 to 4000 sec. For specific impulses of 2000 and 3000 sec, the total accelerating voltage is assumed to be 2000 volts which provides ratios of net to total accelerating voltage of 0.25 and 0.56 respectively. For the specific impulse of 4000 sec, the total accelerating voltage is assumed to be 2500 volts which provides the ratio of net to total accelerating voltage of 0.79. The equations defining total power requirement and thrust are provided in Appendix E. The masses of various subsystems and the power dissipated are calculated by following the methodology of Byers.[27]

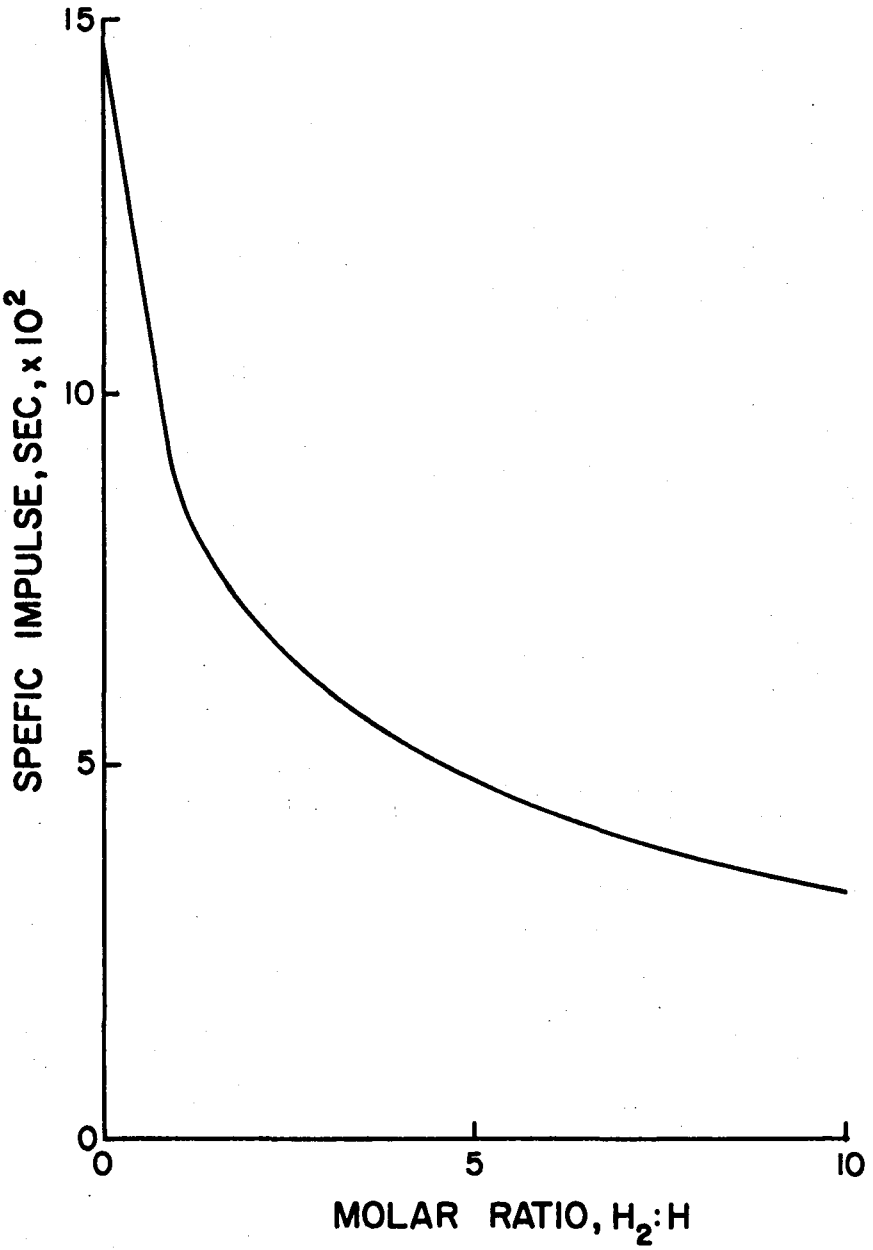

Figure 26. Specific Impulse Versus Molar Ratio of Molecular and Atomic Hydrogen in the Recombination Chamber of Hydrogen Free Radical Thruster.

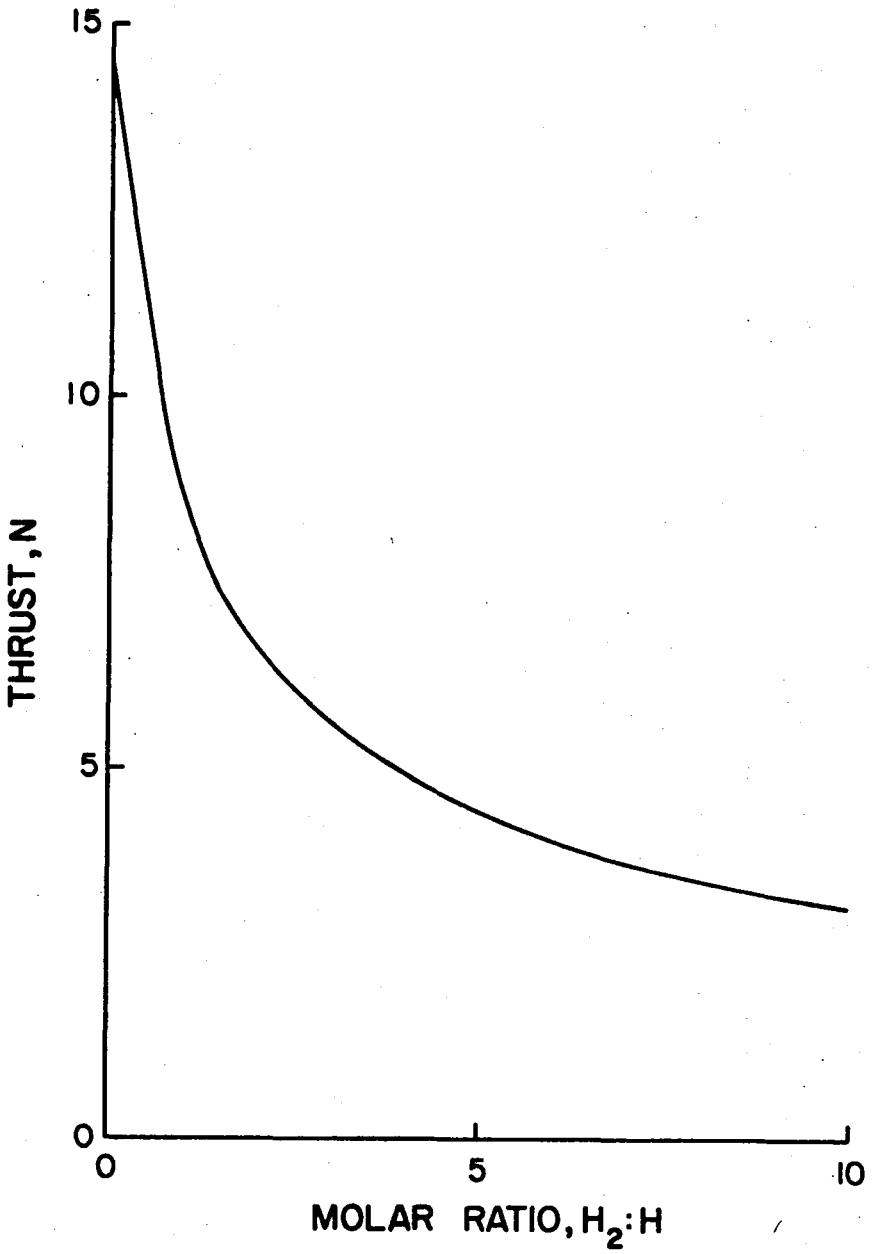

Figure 27. Thrust Versus Molar Ratio of Molecular and Atomic Hydrogen in the Recombination Chamber of Hydrogen Free Radical Thruster.

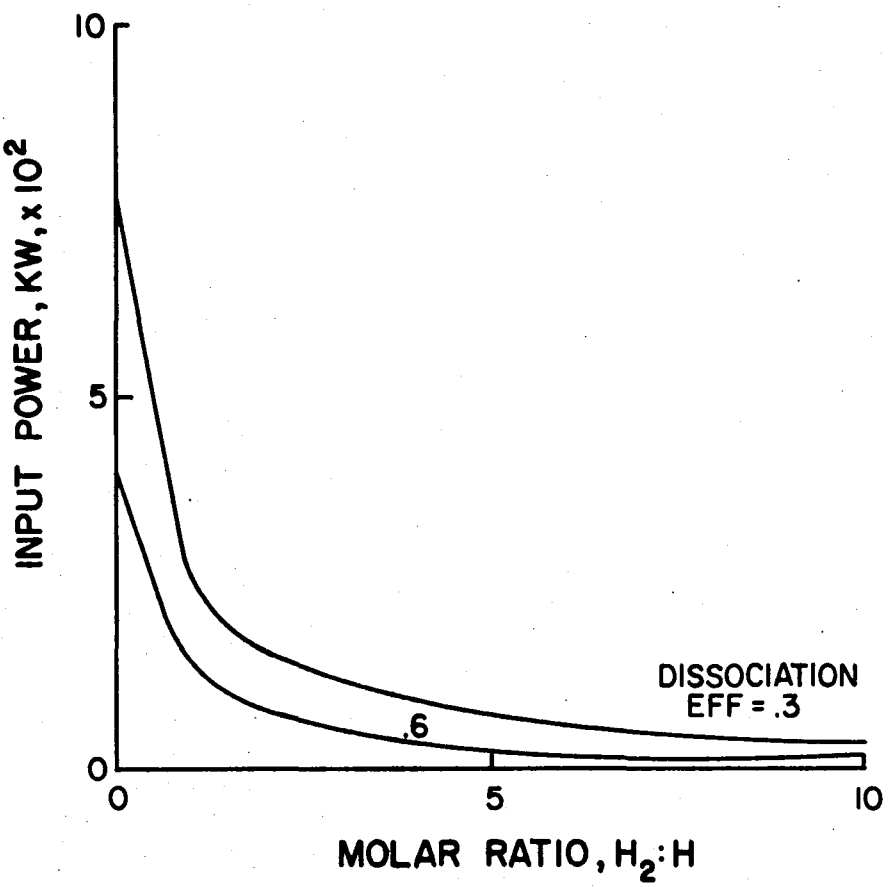

Figure 28. Input Power Versus Molar Ratio of Molecular and Atomic Hydrogen in the Recombination Chamber of Hydrogen Free Radical Thruster.

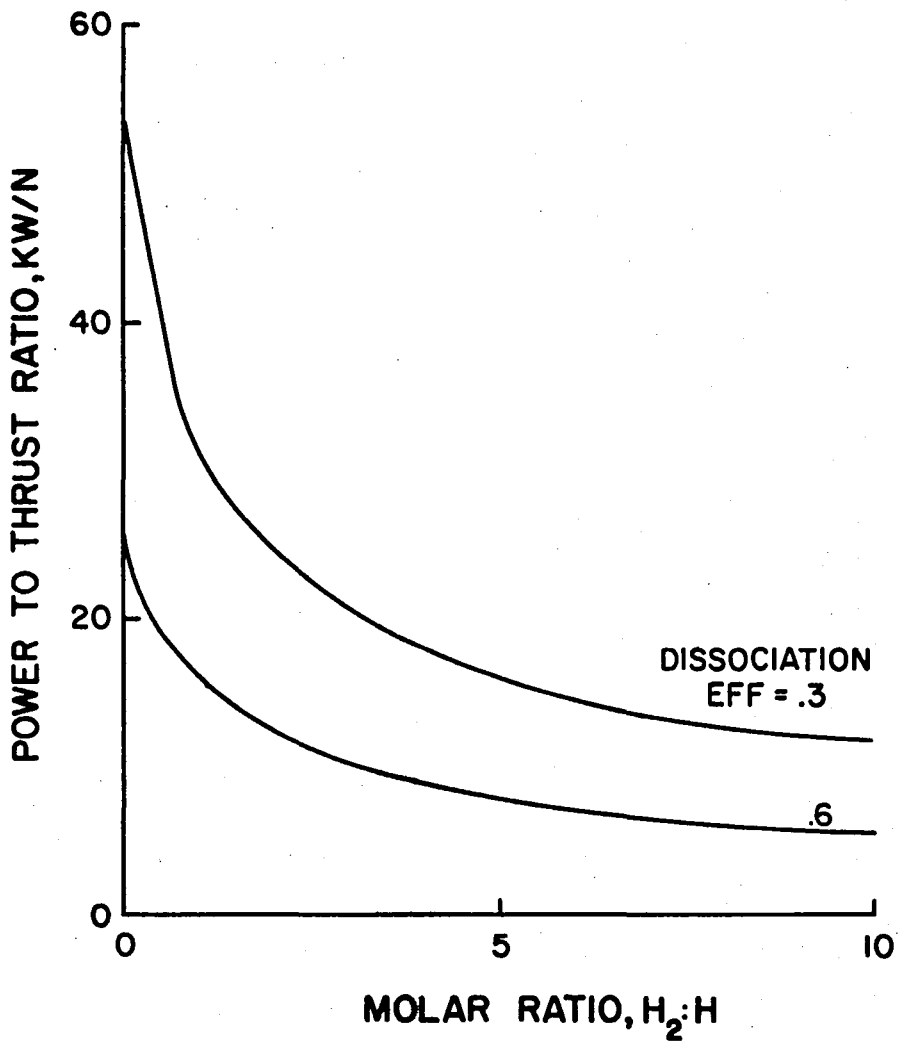

Figure 29. Power to Thrust Ratio Versus Molar Ratio of Molecular and Atomic Hydrogen in the Recombination Chamber of Hydrogen Free Radical Thruster.

Overall efficiency of the ion engine is presented in Fig. 30 against specific impulse. These thrusters operate at quite high efficiencies, 55 percent to 68 percent for the range of specific impulses concerned. The input power requirement is tens of kilowatts (Fig. 31) and the thrust developed is a few newtons (Fig. 32). Dry system mass is shown in Fig. 33. Figure 34 provides the power to thrust ratio which ranges from 18 to 30 kw/N. Thrust to dry weight ratio remains practically constant at 2×10^{-4} (Fig. 35).

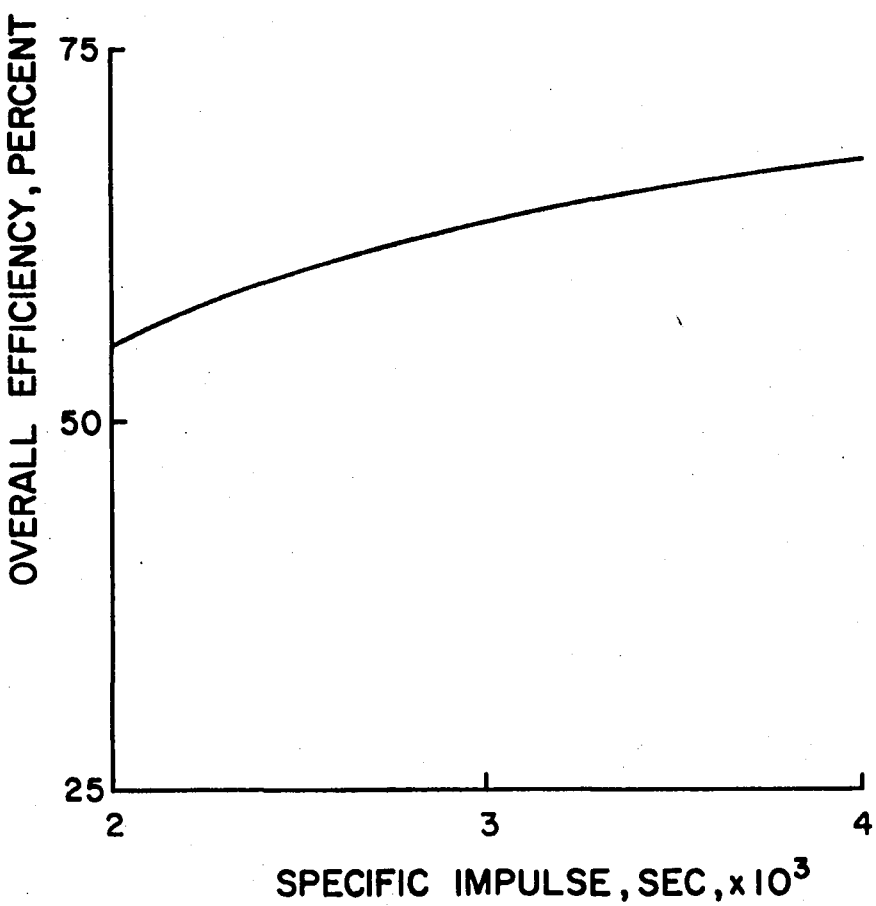

Figure 30. Effect of Specific Impulse on Overall Efficiency of Mercury Ion Engine.

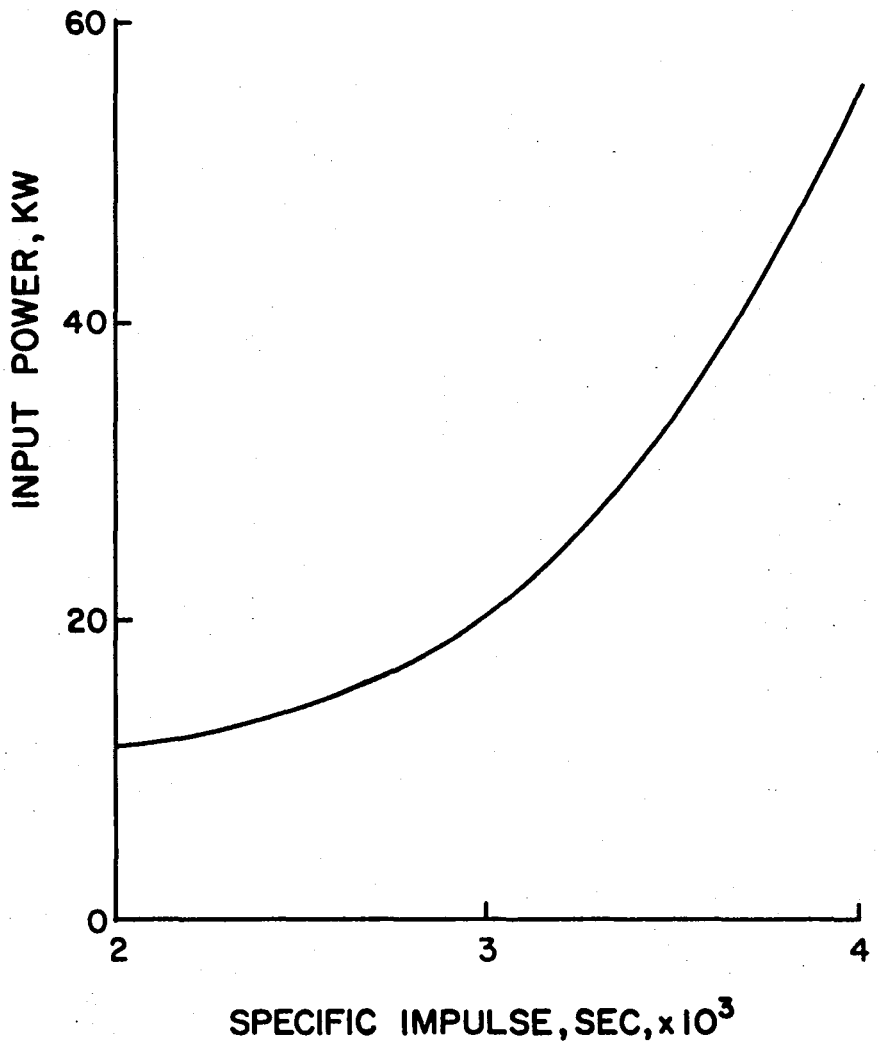

Figure 31. Effect of Specific Impulse on Input Power of Mercury Ion Engine.

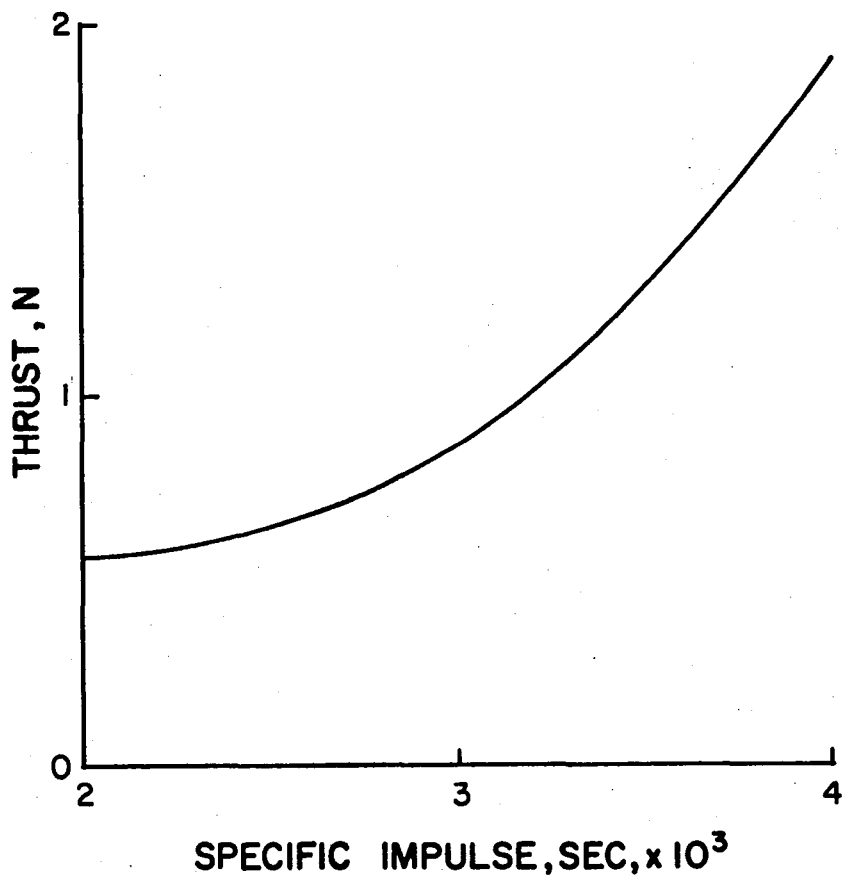

Figure 32. Effect of Specific Impulse on Thrust of Mercury Ion Engine.

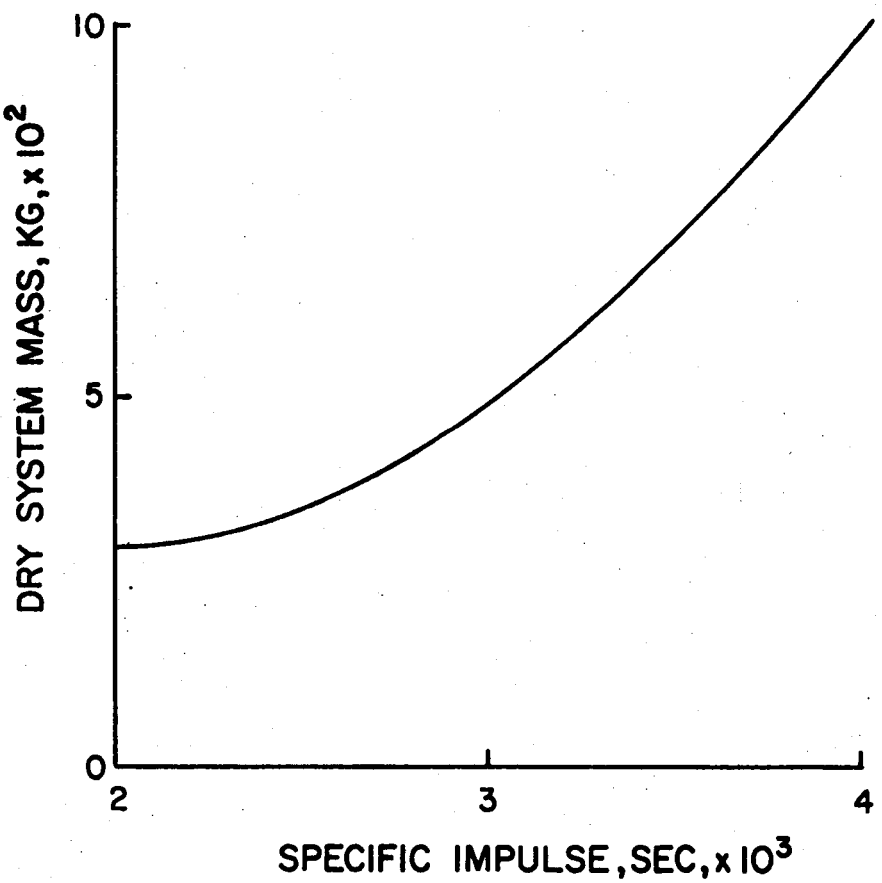

Figure 33. Effect of Specific Impulse on Dry System Mass of Mercury Ion Engine.

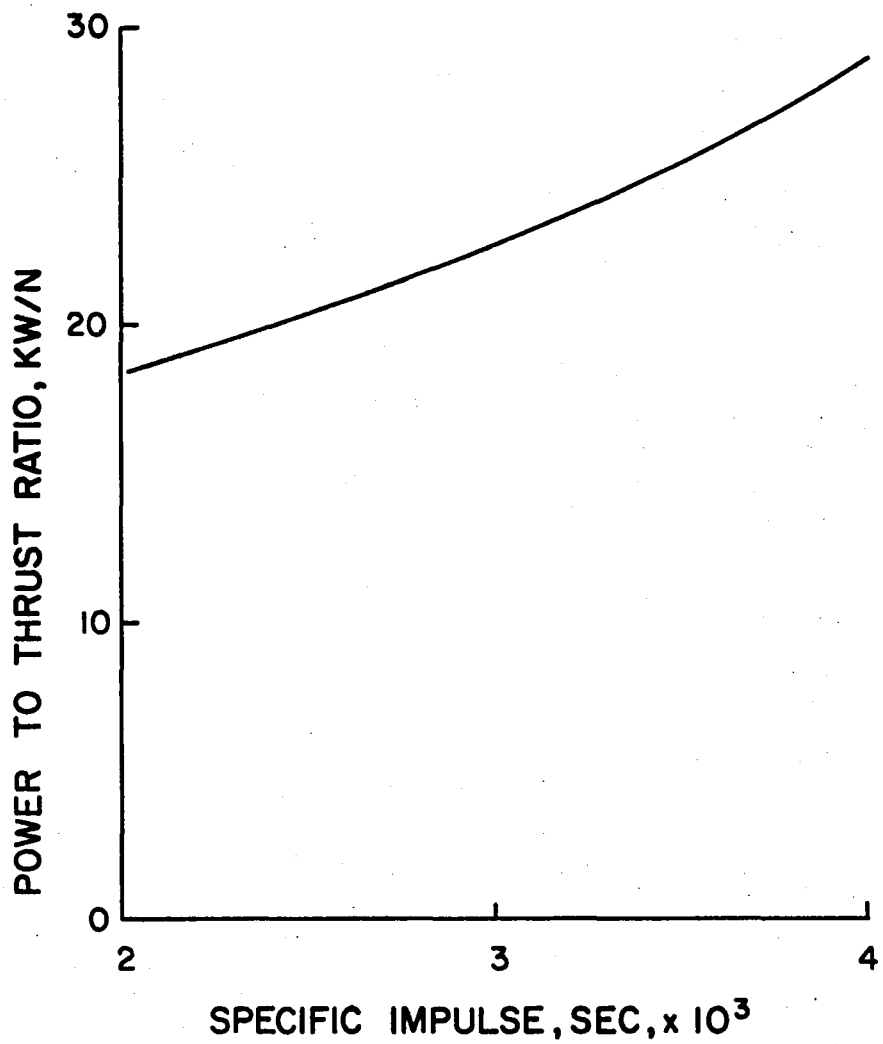

Figure 34. Power to Thrust Ratio of Mercury Ion Engine Versus Specific Impulse.

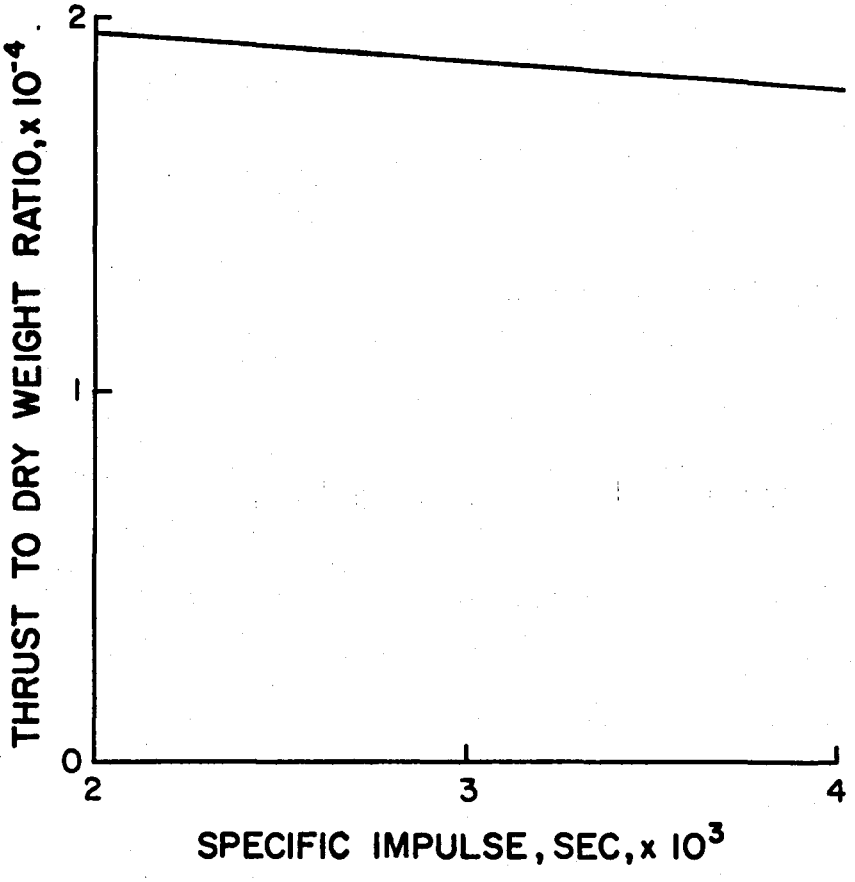

Figure 35. Thrust to Dry Weight Ratio of Mercury Ion Engine Versus Specific Impulse.

COMPARATIVE EVALUATION

The five electric propulsion systems are compared on the basis of four parameters; specific impulse, overall efficiency, power to average thrust ratio and average thrust to dry weight ratio. Two of these parameters are most important in characterizing any rocket propulsion system, specific impulse and overall efficiency. The specific impulse signifies how effectively the fuel is being utilized. Overall efficiency has a considerable effect on the total mass of the propulsion system, through power plant and radiator masses, which in turn affect the payload capacity of the spacecraft.

Each type of electric propulsion system can be operated over a certain range of specific impulse. The characteristics of mass drivers have been calculated for specific impulses varying from 1000 to 1500 sec, but even at I_{sp} = 1000 sec, this type of propulsion system demands a power of several megawatts. Since, the efficiency of rail guns decreases as the specific impulse is increased, rail gun characteristics have been calculated for I_{sp} = 1000 sec to I_{sp} = 2000 sec.

Due to their ability to accelerate macroparticles, both mass drivers and rail guns can produce relatively high average thrusts (tens to hundreds of newtons). Hence, the average thrust densities of these two propulsion systems are high, from 10^5 to 10^6 N/m^2. Thus, mass drivers and rail guns are basically high power, high thrust devices.

From the experimental data of the benchmark MPD thruster before the onset of voltage fluctuations, it can be seen that the maximum specific impulse is 2200 sec. In hydrogen free radical thrusters it is expected to stay below 1500 sec. Only ion engines can operate well

beyond this range, from 2000 to 4000 sec. All of these thrusters produce low thrusts (~ newtons) and require low input power (hundreds of kilowatts). Thrust densities in these devices are several hundred newtons per square meter.

Overall efficiencies of the five electric propulsion systems are shown in Fig. 36 against specific impulse. For mass drivers, overall efficiency is plotted on the basis of a projectile mass of 15 gm whereas for rail guns, it is plotted for a projectile mass of 0.5 gm. For MPD thrusters, overall efficiency presented is for a current pulse of 15 KA.

Mass drivers are found to have the highest efficiency of all electric propulsion systems. However, these efficiency values may be too optimistic, because for such a small size linear accelerator, the energy losses are expected to be higher than those obtained from the equations provided in Appendix A. Rail guns are observed to have low efficiencies due to large amounts of energy loss in the rails. There is an appreciable amount of power loss associated with the electromagnetic plasma acceleration process which currently makes the MPD devices a low efficiency thruster. Dissociation efficiency of hydrogen molecules in free radical thrusters has been arbitrarily assumed in this study and for a dissociation efficiency of 0.6, the overall efficiency of free radical thrusters is 27 percent. Ion engines operate at reasonably high efficiencies because electrostatic acceleration of ions is essentially a loss free process.

Power to average thrust ratios are presented in Fig. 37 against specific impulse. Mass drivers are found to have the lowest power to thrust ratio among all electric propulsion systems. Rail guns and MPD

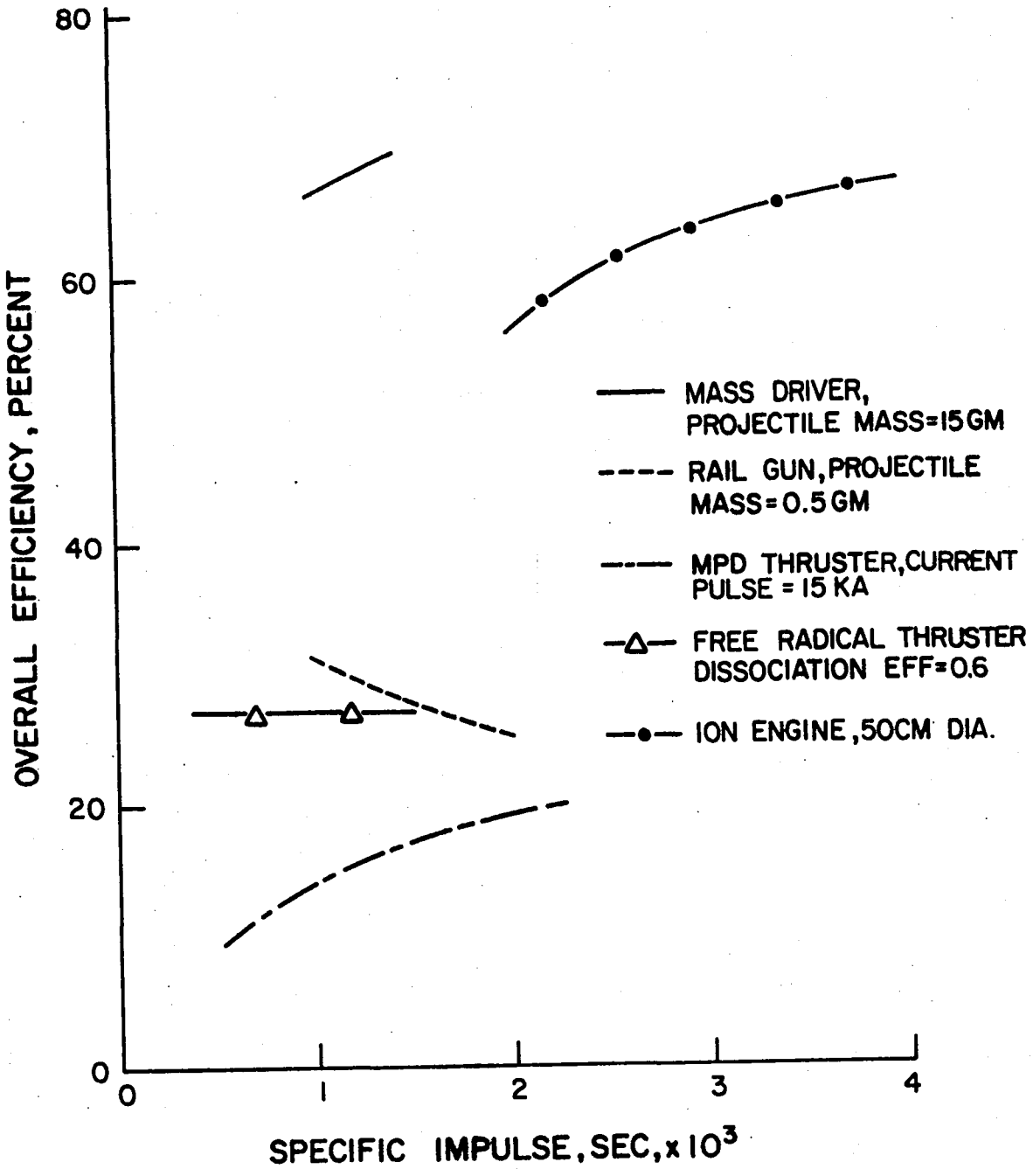

Figure 36. Overall Efficiency of Electric Propulsion Systems Versus Specific Impulse

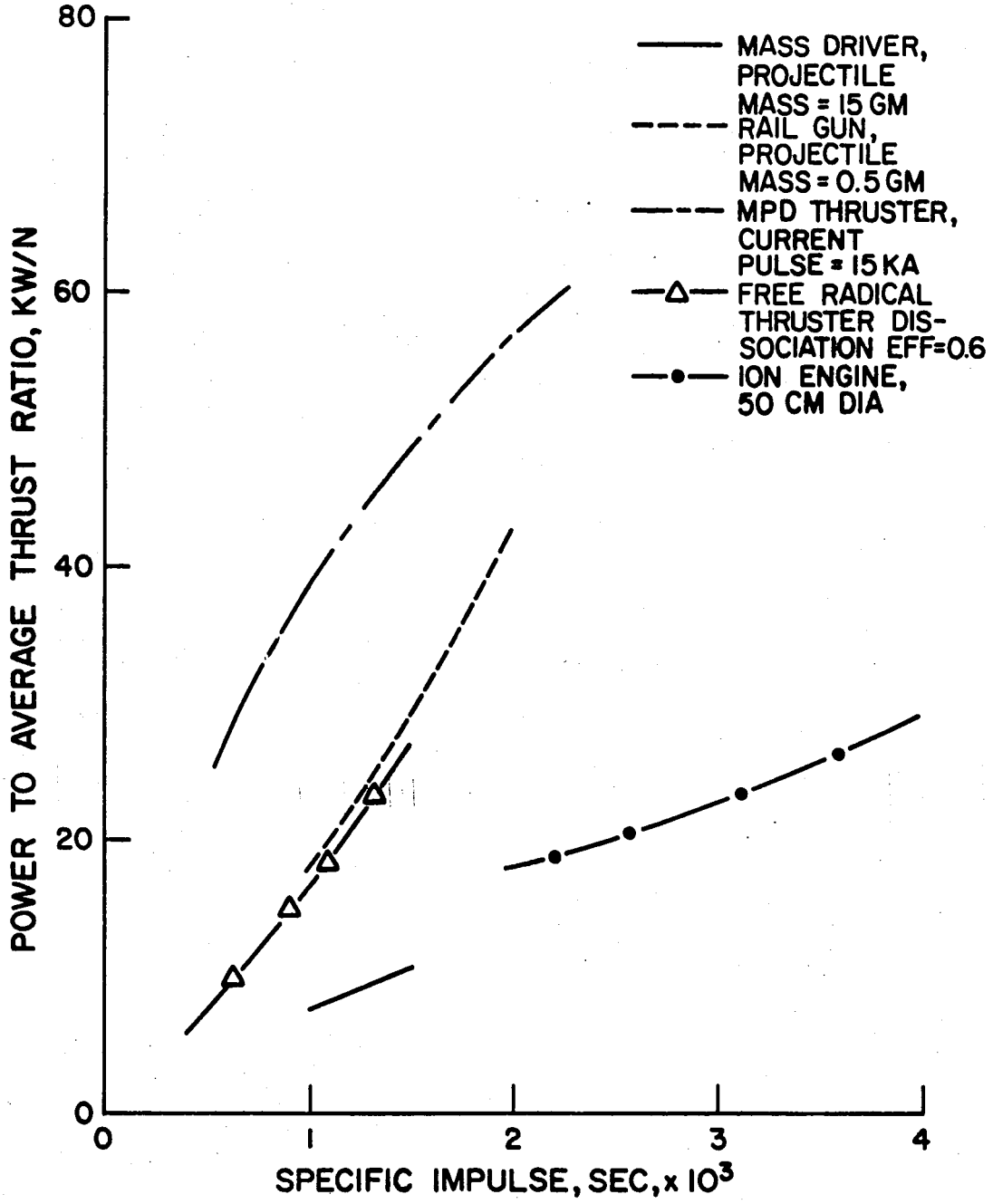

Figure 37. Power to Average Thrust Ratio of Electric Propulsion Systems Versus Specific Impulse

thrusters have relatively high power to average thrust ratios due to their low efficiencies. Free radical thrusters also have a high power to thrust ratio if a large percentage of H_2 can be dissociated in the plasma cavity i.e., if they can be operated at a high specific impulse. Power to thrust ratio of ion engines is low although it operates at considerably higher specific impulses.

Average thrust to dry weight ratio is shown in Fig. 38 for mass drivers, rail guns and ion engines. Mass drivers have the highest thrust to dry weight ratio followed by ion engines and rail guns. Thrust to dry weight ratios of MPD thrusters and free radical thrusters could not be determined due to insufficient design information about these thrusters.

Among the electric propulsion systems evaluated, only the ion engine is flight qualified and ready for a mission. Mass drivers and free radical thrusters are currently in various experimental stages to verify the basic technical concepts. Rail guns and MPD thrusters are in a more advanced development stage having accumulated a large body of experimental data in several laboratories. These electric propulsion systems have to go through an enormous number of development stages, from component development and performance verification to systems engineering studies and reliability testing.

Mass driver characteristics in terms of overall efficiency, power to average thrust ratio and average thrust to dry weight ratio are the best of all electric propulsion systems. Work is currently in progress for improved designs of this type of electromagnetic accelerators.[30] However, due to limitations of current, acceleration of the projectiles in these systems is restricted to about 10^3 g's. Thus, a very large

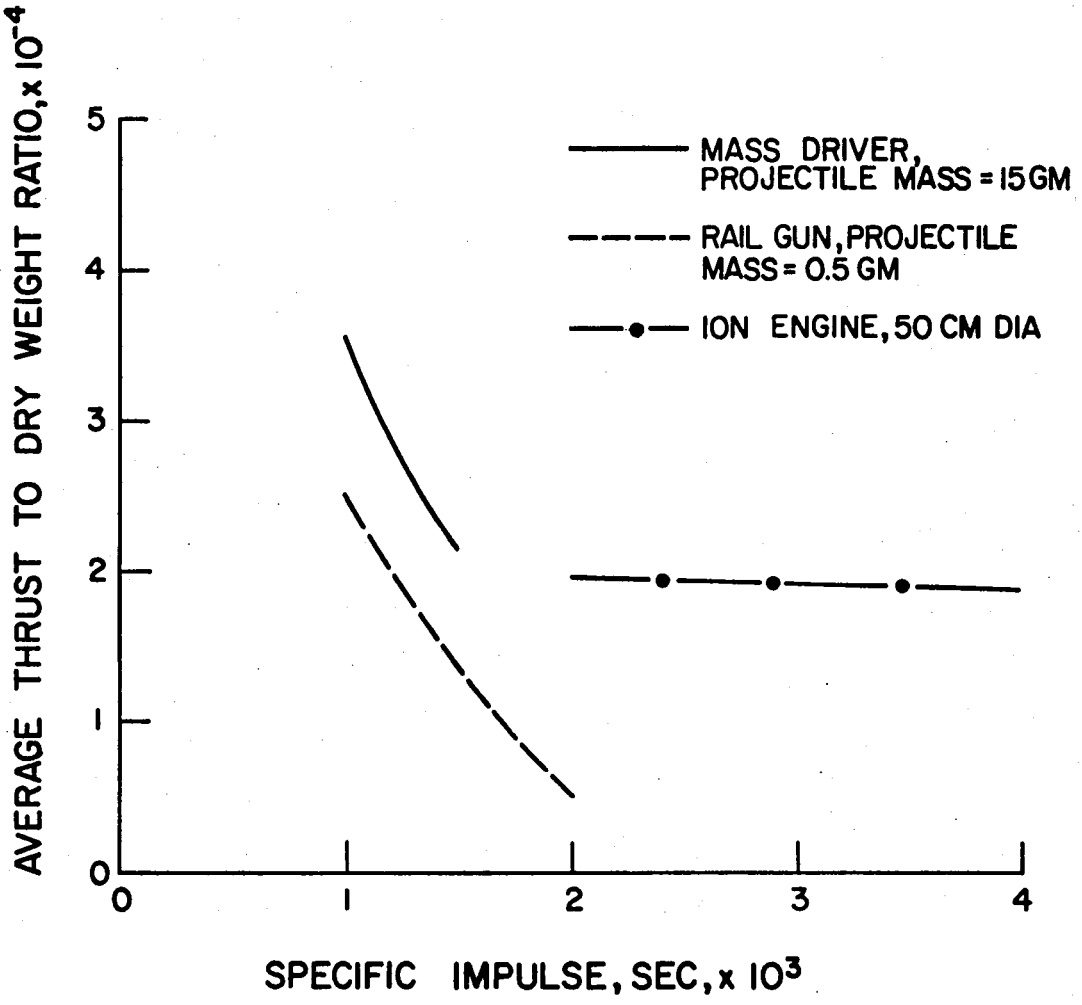

Figure 38. Average Thrust to Dry Weight Ratio of Mass Driver, Rail Gun and Ion Engine Versus Specific Impulse

length launcher (several kilometers) is required to attain a velocity of the projectile to deliver a specific impulse of at least 1000 sec. This limitation in accelerator length is overcome in rail guns where projectiles are capable of achieving very high acceleration ($\sim 10^5$ g's). Thus, practical length accelerators (tens of meters) can be used to launch reaction masses. However, rail guns are currently characterized by low efficiencies and hence, high power to thrust ratios.

The MPD thrusters also have quite low efficiencies. The power to thrust ratios of these thrusters are consequently high. However, there are indications that the characteristics of the MPD thrusters can be improved as development work continues. By replacing the 10 cm diameter anode orifice of the benchmark thruster with one of 6 cm diameter, the specific impulse was increased to 3000 sec and the thruster efficiency was increased to over 30 percent.[8]

The efficiency of dissociation of H_2 in a plasma cavity is extremely low. In recent experiments, dissociation efficiencies ranging from 1.5 to 6.0 percent have been observed.[25] Thus, this type of propulsion system has a long way to go before it be comes viable.

The mercury ion engines offer reasonably high efficiencies. The thrust to dry weight ratio of these devices are comparable to those of mass drivers. The power to thrust ratios of ion engines are somewhat higher than those of mass drivers. Yet these values are low enough despite the fact that ion engines operate at considerably higher specific impulses. Ion engines do not have the drawbacks of mass drivers of a large power requirement or of an exceedingly large length. Although, they produce low thrusts, several of them can be put together in a

module to provide higher thrust. In view of these, it is concluded that overall, ion engines have somewhat better characteristics as compared to the other electric propulsion systems.

CONCLUSIONS

Of the five electric propulsion systems evaluated, mass driver, rail gun and MPD thruster are impulsive devices whereas free radical thruster and ion engine are continuous thrust devices. Mass driver and rail gun are capable of producing high average thrusts. Consequently, their input power requirements are rather high. In contrast, MPD thruster, free radical thruster and ion engine produce low thrust and hence, have low input power requirements.

Rail gun, MPD thruster and free radical thruster are currently characterized by low efficiencies. Mass drivers are found to be the highest efficiency converters of electrical to kinetic energy. However, even for a small size (5 cm dia) and a low specific impulse (1000 sec), the required length of a mass driver is several kilometers.

Among the electric propulsion systems studied, only the ion engine can operate at a specific impulse beyond 2000 sec. The maximum value of the specific impulse up to which the other electric propulsion systems can be operated is apparently limited to about 2000 sec.

Mercury ion engines have demonstrated relatively high efficiencies at low power to thrust ratios while operating at high specific impulses. Given the advanced state of technological development of ion engines combined with their excellent operating characteristics, they have an edge over the other electric propulsion systems.

REFERENCES

1. Disher, J. H., "Next Steps in Space Transportation and Operations," Astronautics and Aeronautics, 16, 22 (January 1978).

2. Bekey, I., "Big Comsats for Big Jobs at Low User Cost," Astronautics and Aeronautics, 17, 42 (February 1979).

3. Disher, J. H., "Space Transportation, Satellite Services and Space Platforms," Astronautics and Aeronautics, 17, 43 (April 1979).

4. Kerslake, W. R. and Ignaczak, L. R., "Sert II 1980 Extended Flight Thruster Experiments," NASA Technical Memorandum 81685 (1981).

5. Chilton, F. et al., "Mass-Driver Applications," Prog. in Astronautics, 57, 63 (1977).

6. Barber, J. P., "Electric Rail Gun Application to Space Propulsion," AIAA Paper No. 79-2091 (1979).

7. Hugel, H., "Self-Magnetic Effect in Arcjet Engines," AIAA Journal, 6, 1573 (1968).

8. Burton, R. L. et al., "Thrust and Efficiency of a Self-Field MPD Thruster," AIAA Paper No. 81-0684 (1981).

9. Hawkins, C. E. and Nakanishi, S., "Free Radical Propulsion Concept," NASA Technical Memorandum 81770 (1981).

10. Fearn, D. G., "The Application of Ion Propulsion to the Transportation and Control of Solar Power Satellites," AIAA Paper No. 81-0760 (1981).

11. Chilton, F. et al., "Electromagnetic Mass Drivers," Prog. in Astronautics, 57, 37 (1977).

12. O'Neill, G. K., "Mass Driver Reaction Engine as Shuttle Upper Stage," Space Manufacturing Facilities; Space Colonies 2, Proceedings of the 3rd Princeton/AIAA Conference, ed. Jerry Grey, pp. 109 (1977).

13. Snow, W. R. and O'Neill, G. K., "Construction and Testing of the 2.5 m Mass Driver," AIAA Paper No. 79-2095 (1979).

14. Snow, W. R. and Dunbar, R. S., "Mass Driver Reaction Engine Characteristics and Performance in Earth Orbital Transfer Missions," AIAA Paper No. 81-0748 (1981).

15. Marshall, R. A., "The Australian National University Rail Gun Project," Atomic Energy, 1, 18 (1975).

16. Rashleigh, S. C. and Marshall, R. A., "Electromagnetic Acceleration of Macroparticles to High Velocities," J. Appl. Phys., 48, 2540 (1978).

17. Bauer, D. P. et al., "Application of Electromagnetic Accelerators to Space Propulsion," Presented at the Conference on Electromagnetic Guns and Launchers," Nov. 4-6, 1980. San Diego, CA.

18. Bauer, D. P. et al., "Electric Rail Gun Propulsion Study," Report AFRPL-TR-81-02 (1981).

19. Bauer, D. P. et al., "The Electric Rail Gun for Space Propulsion," Report NASA-CR-165312 (1981).

20. Hawke, R. S. et al., "Electromagnetic Rail Gun Launchers: Space Propulsion Applications," AIAA Paper No. 81-0751 (1981).

21. Boyle, M. J. et al., "Flowfield Characteristics and Perofrmance Limitations of Quasi-Steady Magnetoplasmadynamic Accelerators," AIAA Journal, 14, 955 (1976).

22. Rudolph, L. K. et al., "Onset Phenomena in Self-Field MPD Arcjets," AIAA Paper No. 78-653 (1978).

23. King, D. Q. et al., "Effect of Thrust Chamber Configuration on MPD Arcjet Performance," AIAA Paper No. 79-2051 (1979).

24. Kuriki, K. et al., "Flight Performance Test of MPD Thruster System," AIAA Paper No. 81-0664 (1981).

25. Chapman, R. et al., "Microwave Plasma Generation of Hydrogen Atoms for Rocket Propulsion," AIAA Paper No. 81-0675 (1981).

26. Etters, R. D. and Flurchik, K., "Atomic Hydrogen Rocket Engine," AIAA Paper No. 81-0677 (1981).

27. Byers, D. C. et al., "Primary Electric Propulsion for Future Space Missions," NASA Technical Memorandum 79141 (1979).

28. Byers, D. C., "Characteristics of Primary Electric Propulsion Systems," NASA Technical Memorandum 79255 (1979).

29. Byers, D. C., "Upper Stages Utilizing Electric Propulsion," NASA Technical Memorandum 81412 (1980).

30. O'Neill, G. K. et al., "High Performance Mass Drivers," AIAA Paper No. 81-0749 (1981).

31. Stewart, P. A. E., "Liquid Hydrogen as a Working Fluid in Advanced Propulsion Systems," British Interplanetary Society Journal, 18, 225 (1961).

32. Szego, G. C., "Similitudes and Limitations in Trans-Conventional Propulsion Systems," Presented at 9th International Astronautical Congress, Amsterdam, pp. 421 (1958).

APPENDIX A

Axial Mass Driver

An axially symmetric mass driver with a four-coil carrier is considered in this study.[12] The nominal diameter of the drive winding is 5 cm. The parameters of the mass driver are listed in Tables 1 and 2.

At a current density of 25,000 amp/cm^2 in the superconducting coils of the carrier, total carrier mass is estimated to be 22 gm. The axial force, F_x, on the bucket is found to be 180 N.

The acceleration, a, of the carrier is

$$a = \frac{F_x}{22 + m} \tag{1}$$

where m is the reaction mass in gm. For a given specific impulse, I_{sp}, the exhaust velocity, V_{max}, is given by

$$V_{max} = 9.81\ I_{sp} \tag{2}$$

The length of the accelerator section, S_a, is

$$S_a = \frac{(V_{max})^2}{2a} \tag{3}$$

and the length of the decelerator section, S_d, is

$$S_d = S_a \cdot \frac{22}{22 + m} \tag{4}$$

The total length of the mass driver, S_{tot}, is

$$S_{tot} = S_a + S_d \tag{5}$$

Table 1

Mass Driver Design Parameters

R	Radius of drive winding	2.5 cm
r	Radius of driven coil (0.53 R)	1.33 cm
l_p	Distance between coils carrying in-phase currents (2.5 R)	6.3 cm
n_2	Number of turns per drive winding	8
i_d	Peak drive current	7,580 amp-turns
l_w	Circumference of drive winding	15.9 cm
L_w	Inductance per winding	0.165 μH
n_C	Number of sine wave excitation cycles undergone by each drive coil	4
n_w	Number of drive coils simultaneously connected to each sector capacitor bank	4
F_x	Axial force on bucket	180 N

Table 2

Geometry-Independent Mass Driver Parameters

ρ_R	Resistivity of winding	2.81×10^{-8} Ω - m
ρ_{kg}	Density of winding	2,800 kg/m^3
m_S	Specific mass of SCR	5×10^{-9} kg/volt-amp
m_C	Specific mass of capacitor	8×10^{-3} kg/Joule
m_P	Specific mass of power plant	10 kg/kw
m_R	Specific mass of radiator	10 kg/kw

The total mass of the silicon-controlled rectifiers, M_s, is given by

$$M_s = 8\pi \left(\frac{i_d}{l_p}\right)^2 S_{tot} V_{max} L_w \frac{m_s}{f_m} \tag{6}$$

where f_m is the ratio of (V_{max}/l_p) to the resonant LC frequency. The total mass of windings and the masses of power supplies and radiators associated with their losses is minimized with respect to the cross-sectional area of the winding, A_{do}. The optimum value of A_{do} is

$$A_{do} = \left[\frac{n_c l_p f_R f_m i_d^2 \rho_R (m_p + m_R)}{4 V_{max} \rho_{kg}}\right]^{1/2} \tag{7}$$

and is reached at equal masses for the windings and those of their associated power supplies and radiators. The total mass of winding, M_w, is

$$M_w = 12 S_{tot} l_w A_{do} \rho_{kg} / l_p \tag{8}$$

The total mass of capacitors and feeders and the masses of power supplies and radiators associated with their losses is minimized simultaneously with respect to sector length, l_s, and feeder conductor cross-sectional area, A_{fo}. The optimum value of A_{fo} is

$$A_{fo} = \left[\frac{n_w^3 L_w i_d^4 m_c \rho_R f_R f_m (m_p + m_R)}{128\, n_2^2 \rho_{kg}^2 V_{max}}\right]^{1/3} \tag{9}$$

and is reached at equal masses for the three components. The total mass of each of the three components, M_c, when minimized is

$$M_c = 12\, A_{fo} S_{tot} \rho_{kg} \tag{10}$$

The average thrust, T, and the average kinetic power output, P_o, in the exhaust beam are given by,

$$T = f_R m V_{max} \tag{11}$$

and

$$P_o = \frac{1}{2} f_R m V_{max}^2 \tag{12}$$

The average power radiated is calculated by dividing the total power and radiator masses by the sum of power plant and radiator specific masses. The average power input is the sum of average kinetic power output and the average power radiated. In the absence of design data, the mass of the power conditioning system is assumed to be 5 kg per kilowatt of input power and the bucket return passageway mass is assumed to be 2 kg per kilowatt of input power. The efficiency of the power conditioning system is taken to be 0.9. The overall efficiency is calculated by dividing the average power output in the exhaust beam by the power output of the power plant.

APPENDIX B

Rail Gun Thruster

The correlations developed by Bauer et al. are used to calculate the characteristics of rail gun thrusters.[19] For a given projectile mass, m, and exhaust velocity, v, the efficiency of the accelerator, η_a, is approximated by

$$\eta_a = 1.367\ m^{0.104} v^{-0.299} \tag{1}$$

where m is in kg and v is in km/sec. The projectiles are assumed to be made of a composite of resin and graphite fibers having a density of 2,200 kg/m^3 to withstand extremely high accelerating stresses. It is further assumed that the projectile thickness is half the bore width, H. For a square bore rail gun, H is then

$$H = \left(\frac{2m}{2200}\right)^{1/3} \tag{2}$$

The optimum length of the rail gun, X, is correlated to the bore width and exhaust velocity by,

$$X = 45.6\ Hv^2 \tag{3}$$

where H is in meters. The current, I, required to accelerate the projectiles to the required exhaust velocity is

$$I = \left(\frac{2ma}{L}\right)^{1/2} \tag{4}$$

where a is acceleration of the projectile and L is the inductance gradient of the rails and assumed to be 0.4×10^{-6} Henry/meter. The acceleration, a, is

$$a = \frac{v^2}{2X} \tag{5}$$

The average thrust, T, and the average power output in the exhaust beam, P_o, are given by,

$$T = f_R mv \tag{6}$$

and

$$P_o = f_R \left(\frac{mv^2}{2}\right) \tag{7}$$

where f_R represents number of projectiles launched per second. The average power input, P_{in}, is

$$P_{in} = \frac{P_o}{\eta_a \eta_{ps}} \tag{8}$$

where η_{ps} is the efficiency of the power conditioning system and assumed to be 0.9. The overall efficiency of the rail gun, η, is

$$\eta = \eta_a \eta_{ps} \tag{9}$$

The mass of the accelerator M_a, is correlated by

$$M_a = 1.17 \times 10^2 mv^2 + 2.99 \times 10^{-6} m^{5/6} (v \times 1000)^{5/2} \tag{10}$$

where m is in kg, v is in km/sec and M_a is in kg. The power conditioning system mass is assumed to be 5 kg per kilowatt of input power and the pellet handling system mass is assumed to be 1 kg per kilowatt of input power. The radiator and power plant specific masses are taken to be 10 kg/kw each.

APPENDIX C

MPD Thruster

The empirical relationships developed for the benchmark argon MPD thruster at Princeton University are used here.[8] The thrust, T, is correlated by

$$T = bJ^2 \tag{1}$$

where J is the current pulse in amperes and b is a proportionality constant given by

$$b = 1 \times 10^{-7}\left[\ln\left(\frac{0.011\ J^2}{\dot{m}} + 5.63\right)\right] \tag{2}$$

In equation 2, J is in kiloamperes and $\dot{m}$ is the argon mass flow rate in gm/sec. The specific impulse, I_{sp}, and the thruster efficiency, η_t, are given by,

$$I_{sp} = \frac{T}{\dot{m}g} \tag{3}$$

and

$$\eta_t = \frac{T^2}{2\dot{m}JV} \tag{4}$$

where V is the terminal voltage. The thrust, T, obtained from equation 1 is impulsive thrust. In this study, we have assumed that the thrust remains steady for a period τ = 1 msec and the cycle time T_c is 10 msec. The average thrust, T_{av}, is then

$$T_{av} = T \cdot \frac{\tau}{T_c} \tag{5}$$

The average power output in the exhaust beam, P_o, is

$$P_o = T_{av} \cdot \frac{v}{2} \tag{6}$$

where v is the velocity of exhaust gases. The average power input, P_{in}, is

$$P_{in} = \frac{P_o}{\eta_t \eta_{ps}} \tag{7}$$

where η_{ps} is the efficiency of the power conditioning system and assumed to be 0.9. The overall efficiency of the MPD thruster, η, is

$$\eta = \eta_t \eta_{ps} \tag{8}$$

APPENDIX D

Free Radical Thruster

For the hydrogen free radical thruster, the amount of energy released due to 100% dissociation and recombination is 51.21 kcal per gm of gas flow.[31] However, if only a fraction of the H_2 gas flow is dissociated, then the energy released due to recombination of all of the atomic hydrogen will be less than 51.21 kcal per gm of gas flow. Table 1 lists the energy released, ΔH, from several free radical molar compositions, H_2:H, assuming 100% efficiency in recombination.

All of the energy released due to recombination of free radicals can not be converted into the kinetic energy of the ejected matter. A large portion of the energy of the exhaust gases leaves the nozzle as residual enthalpy. In this study, we have assumed that 50% of the energy input into the combustion chamber is available for conversion into

Table 1

Hydrogen Free Radical Thruster Parameters

Free radical molar composition (H_2:H) β:1	Energy release, ΔH (kcal per gm of gas flow)	Specific Impulse I_{sp} (sec)	Conversion α
0:1	51.21	1493	1.00
1:1	16.98	860	.33
2:1	10.18	665	.20
5:1	4.62	448	.09
10:1	2.42	325	.05

kinetic energy. Under these conditions, the specific impulse, I_{sp}, of the free radical thruster is given by[32]

$$I_{sp} = 208(\Delta H)^{1/2} \tag{1}$$

where ΔH is the energy available from 100% recombination of the free radicals generated per gm of gas flow. The specific impulses of atomic hydrogen thrusters for several free radical molar compositions are also listed in Table 1. The velocity of exhaust gas, v, the thrust, T, and the power output in the exhaust beam, P_o, are given by

$$v = I_{sp}\, g \tag{2}$$

$$T = \dot{m}v \tag{3}$$

and

$$P_o = \frac{Tv}{2} \tag{4}$$

where $\dot{m}$ is the gas flow rate.

The fraction α of H_2 molar gas flow converted to atomic hydrogen in the dissociation chamber to get the desired free radical molar composition, β:1, can be calculated as follows. For 1 mole of H_2 flow into the dissociation chamber, 2α mole of H is created and $(1 - \alpha)$ mole of H_2 remains in the mixture. The total number of moles in the mixture is $1 + \alpha$ and the H mole fraction is $2\alpha/(1 + \alpha)$. Then

$$\frac{2\alpha}{1 + \alpha} = \frac{1}{\beta + 1}$$

or,

$$\alpha = \frac{1}{2(\beta + 0.5)} \tag{5}$$

Conversion values of α for several free radical molar compositions is provided in Table 1.

The power, P, needed to dissociate a fraction α of H_2 flow rates of $\dot{M}$ mole/sec is

$$P = \frac{C\alpha\dot{M}}{\eta_d} \tag{6}$$

In equation 6, C is the power required to dissociate a flow of 1 mole/sec of H_2 to H and η_d is the efficiency of dissociation of hydrogen molecules by microwave energy. In the absence of adequate information about the design of the dissociation chamber, we have assumed two values of η_d, 0.3 and 0.6, to reflect two possible values of efficiency of the dissociation process. We have further assumed a power conditioning system efficiency of 0.9. The calculations have been performed by assuming a H_2 mass flow rate of 1 gm/sec.

APPENDIX E

Mercury Electron Bombardment Ion Thruster

The performance of ion thrusters is limited by the maximum ion current density and the allowable range of the ratio, R, of net to total accelerating voltages, V_B/V_T, over which a thruster may be operated. This ratio can vary from 0.2 to 0.9. The total accelerating voltage on close spaced accelerating grids is limited to about 3000 volts.

For mercury ion thrusters, the specific impulse, I_{sp}, the total power required, P_T, and the thrust, T, are given by,[27]

$$I_{sp} = 90.3\ V_B^{0.5} \tag{1}$$

$$P_T = 2.57 \times 10^{-9}\ A\left(\frac{V_B}{R}\right)^{2.25}(V_B + 150) \tag{2}$$

and

$$T = 4.9 \times 10^{-9}\ A\ \frac{V_B^{2.75}}{R^{2.25}} \tag{3}$$

where A is the cross sectional area of the accelerator grid. We have assumed the thruster diameter to be 50 cm which is a modest extrapolation of the state-of-art technology.

The mass of the propellant tank is assumed to be 50 kg in all cases. For analysis of power management and control system, the conventional dc configuration is chosen. The masses of various subsystems and the power dissipation were calculated by following the methodology of Byers.[28]

DISTRIBUTION LIST

	Copies
National Aeronautics and Space Administration Washington, DC 20546	
Attn: RS/Mr. Dell Williams, III	1
RTS-6/Mr. Wayne Hudson	1
RTS-6/Mr. Jerome Mullin	1
MT/Mr. Ivan Bekey	1
National Aeronautics and Space Administration Lewis Research Center 21000 Brookpark Road Cleveland, OH 44135	
Attn: Research Support Procurement Section	
Mr. Steve Szabo, MS 501-11	1
Technology Utilization Office, MS 3-19	1
Report Control Office, MS 5-5	1
Library, MS 60-3	2
Mr. N. Musial, MS 500-113	1
Dr. M. Goldstein, Chief Scientist, MS 5-3	1
Mr. F. Terdan, MS 501-7	1
Mr. D. Byers, MS 501-7	1
Mr. W. Kerslake, MS 501-7	30
Mr. H. Allen, MS 7-3	1
National Aeronautics and Space Administration Lyndon B. Johnson Space Center Houston, TX 77058	
Attn: Mr. Hu Davis	1
National Aeronautics and Space Administration Marshall Space Flight Center Huntsville, AL 35812	
Attn: Mr. Jerry P. Hethcoate	1
Mr. John Harlow	1
Mr. Robert Bechtel	1
Research and Technology Division Wright-Patterson AFB, OH 45433	
Attn: (ADTN) Mr. Everett Bailey	1
NASA Scientific and Technical Information Facility P.O. Box 8757 Baltimore, MD 21240	
Attn: Accessioning Dept.	1

	Copies
Case Western Reserve University 10900 Euclid Avenue Cleveland, OH 44106 Attn: Dr. Eli Reshotko	1
DST 1 Ministry of Defence Metropole Building Northumberland Avenue London, WC2 N5BL ENGLAND Attn: Dr. D. G. Fearn	1
United Kingdom Atomic Energy Authority Culham Laboratory Abingdon, Berkshire ENGLAND Attn: Dr. P. J. Harbour Dr. M. F. A. Harison	1 1
National Aeronautics and Space Administration Goddard Space Flight Center Greenbelt, MD 20771 Attn: Mr. W. Isley, Code 734 Mr. A. A. Vetman Dr. David H. Suddeth	1 1 1
COMSAT Laboratories P.O. Box 115 Clarksburg, MD 20734 Attn: Mr. B. Free Mr. O. Revesz	1 1
Comsat Corporation 950 L'Enfant Plaza, SW Washington, DC 20024 Attn: Mr. Sidney O. Metzger	1
Rocket Propulsion Laboratory Edwards AFB, CA 93523 Attn: LKDA/Mr. Tom Waddell LKDH/Dr. Robert Vondra	1 1
DFVLR--Institut fur Plasmadynamik Technische Universitat Stuttgart 7 Stuttgart-Vaihingen Allmandstr 124 West Germany Attn: Dr. G. Krulle	1

	Copies
Giessen University 1st Institute of Physics Giessen, West Germany Attn: Professor H. W. Loeb	1
Jet Propulsion Laboratory 4800 Oak Grove Drive Pasadena, California 91102	
Attn: Dr. Kenneth Atkins	1
Technical Library	1
Mr. Eugene Pawlik	1
Mr. James Graf	1
Mr. Dennis Fitzgerald	1
Dr. Graeme Aston	1
Electro-Optical Systems, Inc. 300 North Halstead Pasadena, California 91107	
Attn: Dr. R. Worlock	1
Mr. E. James	1
Mr. W. Ramsey	1
TRW Inc. TRW Systems One Space Park Redondo Beach, California 90278	
Attn: Dr. M. Huberman	1
Mr. Sid Zafran	1
National Aeronautics and Space Administration Ames Research Center Moffett Field, California 94035	
Attn: Technical Library	1
National Aeronautics and Space Administration Langley Research Center Langley Field Station Hampton, Virginia 23365	
Attn: Technical Library	1
Mr. B. Z. Henry	1
Hughes Research Laboratories 3011 Malibu Canyon Road Malibu, California 90265	
Attn: Mr. J. H. Molitor	1
Dr. R. L. Poeschel	1
Dr. Jay Hyman	1
Dr. J. R. Beattie	1
Dr. W. S. Williamson	1
Dr. H. J. King	1

	Copies
Princeton University Princeton, NJ 08540 Attn: Dean R. G. Jahn Dr. K. E. Clark	 1 1
Boeing Aerospace Co. P.O. Box 3999 Seattle, Washington 98124 Attn: Mr. Donald Grim, M.S. 8K31 Mr. Russell Dod	 1 1
Lockheed Missiles and Space Co. Sunnyvale, California 94088 Attn: Dr. William L. Owens Propulsion Systems, Dept. 62-13	 1
Fairchild Republic Co. Farmingdale, New York 11735 Attn: Dr. Domenic J. Palumbo	 1
Electrotechnical Laboratory 1-1-4, Umezono, Sakura-Mura, Niihari-Gun Ibaraki, Japan Attn: Dr. Katsuya Nakayama	 1
Sandia Laboratories Mail Code 4537 Albuquerque, NM 87115 Attn: Mr. Ralph R. Peters	 1
Ion Tech, Inc. P.O. Box 1388 1807 E. Mulberry Fort Collins, Colorado 80522 Attn: Dr. Gerald C. Isaacson	 1
EG & G Idaho P.O. Box 1625 Idaho Falls, Idaho 83401 Attn: Dr. G. R. Longhurst, TSA-104	 1
The Aerospace Corporation P.O. Box 95085 Los Angeles, CA 90045 Attn: Dr. B. A. Haatunion Mr. A. H. Silva	 1 1

	Copies
Michigan State University East Lansing, MI 48824 Attn: Dr. J. Asmussen Dr. M. C. Hawley	 1 1
General Dynamics Kearney Mesa Plant P.O. Box 1128 San Diego, CA 92112 Attn: Dr. Ketchum	 1
The Aerospace Corporation Space Sciences Lab. P.O. Box 92957 Los Angeles, California 90009 Attn: Dr. Y. T. Chiu	 1
The Takagi Research Laboratory Department of Electronics Kyoto University Yoshidahonmachi Sakyo-ku Kyoto 606 JAPAN Attn: Dr. Toshinori Takagi	 1
Department of Aeronautics Faculty of Engineering University of Tokyo 7-3-1, Hongo, Bunkyo-ku Tokyo, JAPAN Attn: Prof. Itsuro Kimura	 1
Prof. Tom Maul P.O. Box 98182 Tsim Sha Tsui Post Office Kowloon, Hong Kong British Crown Colony	 1
Mr. Susumu Masaki Department of Electronics Tokyo National Technical College No. 1220-2 Kunugida-cha, Hachioji 193 Tokyo, JAPAN	 1
Mr. Curtis Haynes Tektronix Inc. M.S. 50-431 P.O. Box 500 Beaverton, Oregon 97077	 1

	Copies
Prof. Paul Wilbur Mechanical Engineering Department Colorado State University Fort Collins, Colorado 80523	1
Dr. John Barber International Applied Physics Inc. 7546 McEwen Road Dayton, Ohio 45459	1
Dr. Ron Hawke Lawrence Livermore Laboratory Livermore, California 94550	1
Dr. Richard A. Marshall University of Texas Taylor Hall 167 Austin, Texas 78712	1
Prof. Harold R. Kaufman Department of Physics Colorado State University Fort Collins, Colorado 80523	1
Dr. V. V. Zhurin Computing Center of the USSR Academy of Sciences Vavilova 40 117333 Moscow, B-333 USSR	1
Dr. M. Krishnan Department of Applied Physics P.O. Box 2159 Yale Station New Haven, Connecticut 06520	1
Mr. John Brophy G.S. 9lp Martin Marietta Corp. P.O. Box 1681 Vandenburg AFB, CA 93437	1
Lt. Phil Roberts AFRPL/LKDH, M.S. 24 Edwards Air Force Base, CA 93523	1

End of Document